J. Fluid Mech. (2010), *vol.* 652, *pp.* 259–298.
doi:10.1017/S0022112010000054

Fully nonlinear periodic internal waves in a two-fluid system of finite depth

R. CAMASSA[1]†, P.-O. RUSÅS[2], A. SAXENA[3] AND R. TIRON[1]

[1]Department of Mathematics, University of North Carolina, Chapel Hill, NC 27599-3250, USA

[2]Faculty of Computer Sciences, Østfold University College, N-1757 Halden, Norway

[3]Theoretical Division and Center for Nonlinear Studies, Los Alamos National Laboratory, Los Alamos, NM 87545, USA

(Received 18 May 2009; revised 9 September 2009; accepted 27 November 2009)

Periodic travelling wave solutions for a strongly nonlinear model of long internal wave propagation in a two-fluid system are derived and extensively analysed, with the aim of providing structure to the rich parametric space of existence of such waves for the parent Euler system. The waves propagate at the interface between two homogeneous-density incompressible fluids filling the two-dimensional domain between rigid planar boundaries. The class of waves with a prescribed mean elevation, chosen to coincide with the origin of the vertical (parallel to gravity) axis, and prescribed zero period-average momentum and volume-flux is studied in detail. The constraints are selected because of their physical interpretation in terms of possible processes of wave generation in wave-tanks, and give rise to a quadrature formula which is analysed in parameter space with a combination of numerical and analytical tools. The resulting model solutions are validated against those computed numerically from the parent Euler two-layer system with a boundary element method. The parametric domain of existence of model periodic waves is determined in closed form by curves in the amplitude–speed (A, c) parameter plane corresponding to infinite period limiting cases of fronts (conjugate states) and solitary waves. It is found that the existence domain of Euler solutions is a subset of that of the model. A third closed form relation between c and A indicates where the Euler solutions cease to exist within the model's domain, and this is related to appearance of 'overhanging' (multiple valued) wave profiles. The model existence domain is further partitioned in regions where the model is expected to provide accurate approximations to Euler solutions based on analytical estimates from the quadrature. The resulting predictions are found to be in good agreement with the numerical Euler solutions, as exhibited by several wave properties, including kinetic and potential energy, over a broad range of parameter values, extending to the limiting cases of critical depth ratio and extreme density ratios. In particular, when the period is sufficiently long, model solutions show that for a given supercritical speed waves of substantially larger amplitude than the limiting amplitude of solitary waves can exist, and are good approximations of the corresponding Euler solutions. This finding can be relevant for modelling field observations of oceanic internal waves, which often occur in wavetrains with multiple peaks.

† Email address for correspondence: camassa@amath.unc.edu

1. Introduction

Internal waves are an important feature of geophysical fluid dynamics, as stratification is an inherent component of near-equilibrium states of ocean and atmosphere. Because of the relatively low viscosities and small density differences of water and air in each of these environments, energy penalties paid by natural forcing agents such as tides and winds in displacing fluid parcels from equilibrium are also relatively small, which can result in internal wave motion of large amplitudes, as recent improvements in instrumentation and observational techniques in the ocean are continuously revealing (see e.g. the review by Helfrich & Melville 2006). In this paper, we focus on what is possibly the simplest set-up capable of supporting internal wave motion of arbitrary amplitude, that of a two-layer inviscid and incompressible fluid of homogenous densities between plates of infinite horizontal extent. Despite its long history in the literature, it is only somewhat recently that attention has been paid, by experimental and theoretical investigations (see e.g. Grue *et al.* 1999; Craig, Guyenne & Kalisch 2005; Troy & Koseff 2005; Bona, Lannes & Saut 2008), to the large amplitude motion that can be attained in this configuration. Among other findings, these studies have shown that the long-wave assumption in a two-layer system makes it possible to develop models which can describe solitary wave motion of arbitrary amplitude and provide closed form solutions that compare favourably with laboratory experimental data under appropriate circumstances (Camassa *et al.* 2006). While solitary waves are of interest in many practical situations, e.g. in field studies (Duda *et al.* 2004), a more extensive test of model fidelity is offered by the class of periodic travelling wave motion, which includes that of solitary waves as a limiting case. In this study, we examine periodic wavetrain solutions for a class of long-wave asymptotic models developed by Miyata (1985, 1988) and Choi & Camassa (1996, 1999), and establish the parametric range where such solutions can be considered valid approximations to those of the parent Euler equations. This is carried out by a direct comparison with numerical computations of both two-layer and continuous stratification solutions of the Euler equations, through a variety of wave properties, such as wave profiles, fluid velocities, wave speed and amplitude.

Unlike the case of a solitary wave, whose physical parameters can be linked in the form of boundary conditions to a far-field reference configuration of the fluid, a periodic travelling wavetrain admits a richer class of such parameters, generally related to the invariants of motion. Unfortunately, the highly idealized nature of periodicity extending for all space and time does not allow the identification of a preferred (minimal) set of parameters determining a unique periodic wavetrain, given that the physical processes necessary for its generation, as well as the physically necessary transition to boundary or far-field reference states, are neglected in this idealization. This, of course, is an issue that transcends the case of internal waves. The choice of the most convenient physical quantities that determine a given wavetrain already presents itself in the study of periodic irrotational waves at the free surface of a single fluid layer. It is remarkable that for these waves such questions appear to have been settled only relatively recently, and this only in the context of waves symmetric around their crests (see Benjamin 1995 for a proof of a long-standing conjecture on this issue formulated by Benjamin & Lighthill 1954).

With this in mind, in § 2 we solve by quadratures the system of four ordinary differential equations (ODEs) resulting from the travelling wave ansatz. In this process, we collect four integration constants, which are constants of motion in the wave frame. Thus, at least within the realm of these asymptotic models, the minimal number of

physical invariant quantities needed to determine a unique period wavetrain is four. The phase speed of the wave can then be found by specifying some integral property of the wave (e.g. total horizontal momentum) in the lab frame. In § 3, we establish relations between relevant physical quantities associated with the periodic wavetrain and the four constants of integration in the quadrature. A subset of these relations can be chosen to determine the quadrature's constants. In particular, we show that two of these constants can be given a natural physical interpretation in terms of volume fluxes in each layer. The remaining two integration constants reduce, under the assumption of irrotationality, to two conserved quantities for two-layer potential flow related to the Bernoulli constants and the so-called flow force. These are in turn fixed by seeking, e.g. an *a priori* imposed peak-to-trough amplitude and a prescribed mean layer thickness. This choice makes the connection with previous work on solitary waves somewhat more transparent by defining a quiescent state and allows us to follow easily the model solutions in the distinguished limits of infinitesimal wave amplitudes, where the long-wave critical speed is naturally defined from the general Euler internal wave dispersion relation for a two-fluid system (Lamb 1932).

We proceed, in § 4, to construct a particular class of periodic waves which limits to the infinitesimal amplitude waves for the quiescent reference state. The final result is a two-parameter family of periodic solutions (e.g. speed and amplitude which determine the period). In particular, our approach allows us to deal with the technical difficulties posed by the quadrature solution which in general leads to hyperelliptic integrals (as opposed to elliptic integrals as in the case of solitary waves). We study the properties of the periodic solutions of this two-parameter family in § 5. In an effort to establish the limitations on model's validity range through its periodic travelling wave solutions, § 6 presents comparisons with numerically computed solutions of both two-layer and near two-layer continuously stratified periodic travelling wave Euler solutions.

The study of the limiting cases of solitary waves and fronts is fundamental to our construction of periodic solutions and it is interesting in its own right. However, to avoid distraction from the main focus of periodic solutions in our constrained class, we relegate the details of these studies to the appendices. In particular, in Appendix A we sketch the construction of solitary wave solutions on background uniform currents in each layer, useful in a systematic study of various classes of periodic travelling wave solutions of the model as demonstrated in Appendix B. Other choices of constraints determining a unique periodic travelling wave solution have been more popular in the literature. Ultimately the issue of which among these is preferable must be related to the physical process of generation of (locally) periodic travelling wave trains. In this respect, we note the controversy around the concepts of wave momentum and mass drift for surface periodic wave trains in one-layer fluids, which has yet to be settled experimentally (cf. McIntyre 1981; Yih 1997; Monismith *et al.* 2007). We discuss some of these alternatives and their connection to our primary choice in Appendix C.

2. The model equations and travelling wave system

We seek periodic wave solutions of the long-wave strongly nonlinear asymptotic model (in the small parameter $\epsilon = H/L$, where L is a typical horizontal scale of the waves and H is the total thickness of the two layers) derived by Choi & Camassa (1999) for a system of two inviscid and nearly irrotational fluid layers of constant densities under gravity (with $\rho_1 < \rho_2$ for stable stratification); see figure 1. The model assumes only one small parameter, with no restrictions on the amplitude of the interface displacement. We define the interface displacement between the two layers

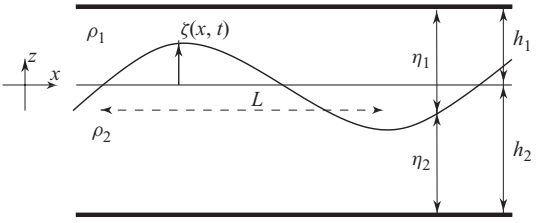

FIGURE 1. Schematics of the two-fluid system with main notation definitions.

as the graph $z = \zeta(x,t)$ and choose the origin of our coordinate systems so that the two fluid layers are bounded above and below by rigid planes at $z = h_1$ and $z = -h_2$, respectively. We denote by $\eta_1(x,t) = h_1 - \zeta(x,t)$ and $\eta_2(x,t) = h_2 + \zeta(x,t)$, respectively, the thicknesses of each layer.

The set of model equations that governs the dynamics of a two-layer system under the long-wave approximation is

$$\eta_{kt} + (\eta_k \overline{u}_k)_x = 0, \tag{2.1}$$

$$\overline{u}_{kt} + \overline{u}_k \overline{u}_{kx} + g\zeta_x = -\frac{1}{\rho_k}\partial_x P_I + \frac{1}{\eta_k}\partial_x\left(\frac{1}{3}\eta_k^3 G_k\right), \quad k = 1\,,2, \tag{2.2}$$

where $\overline{u}_k(x,t)$ denote the layer mean velocities

$$\overline{u}_k(x,t) = \frac{1}{\eta_k}\int_{[\eta_k]} u_k(x,z,t)\mathrm{d}z, \tag{2.3}$$

where the layer domains $[\eta_k]$ are defined as $\zeta \leqslant z \leqslant h_1$ and $-h_2 \leqslant z \leqslant \zeta$, for $k = 1, 2$ respectively, $P_I(x,t)$ is the pressure at the interface, and the nonlinear dispersive terms are defined, respectively, by

$$G_k\,(x,t) = \overline{u}_{kxt} + \overline{u}_k\overline{u}_{kxx} - (\overline{u}_{kx})^2\,, \qquad k = 1, 2. \tag{2.4}$$

The first pair is exact and is simply an expression of mass conservation per layer, while the second pair corresponds to horizontal momentum balance and is accurate up to terms in the long-wave parameter asymptotics of order $O(\epsilon^4)$. For details of the model derivation, see Choi & Camassa (1999).

2.1. *Travelling wave solutions*

For a stationary wave moving from left to right with constant speed (c), we make the change of variable

$$X = x - c\,t\,, \qquad \text{hence} \qquad \partial_t = -c\,\partial_X, \quad \partial_x = \partial_X$$

and consider

$$\zeta(x,t) \equiv \zeta(X), \qquad \overline{u}_k(x,t) \equiv \overline{u}_k(X), \qquad P_I(x,t) \equiv P_I(X). \tag{2.5}$$

The equations of mass conservation and momentum for each layer therefore reduce to a system of four ODEs with respect to the independent variable X. The system can be integrated by quadratures, which introduces four integration constants that represent an equal number of motion invariants. Equation (2.1) becomes, after one integration in X,

$$-c\eta_k + \eta_k\overline{u}_k = C_k, \quad k = 1, 2, \tag{2.6}$$

where C_1 and C_2 are clearly the volume fluxes in the wave frame, in each layer. Eliminating the pressure between the two momentum equations (2.2) and with the

help of (2.6), we obtain

$$\left[\frac{\rho_1 C_1^2}{\eta_1^3}+\frac{\rho_2 C_2^2}{\eta_2^3}-\gamma\right]\zeta_X=\frac{\rho_1}{\eta_1}\left(\frac{1}{3}\eta_1^3 G_1\right)_X-\frac{\rho_2}{\eta_2}\left(\frac{1}{3}\eta_2^3 G_2\right)_X, \tag{2.7}$$

with $\gamma \equiv g(\rho_2-\rho_1)$. In order to separate variables, we integrate the third-order ODE (2.7) once directly and once with the integrating factor η_1, collecting two more constants of integration (which we denote by C_3, C_4, respectively). By eliminating the common second derivative ζ_{XX} between the resulting equations, we obtain the following nonlinear ODE for the interfacial displacement $\zeta(X)$:

$$\zeta_X^2=3\frac{\rho_1 C_1^2\eta_2+\rho_2 C_2^2\eta_1-\gamma\zeta^2\eta_1\eta_2+2C_3\eta_1^2\eta_2-2C_4\eta_1\eta_2}{\rho_1 C_1^2\eta_2+\rho_2 C_2^2\eta_1}. \tag{2.8}$$

This quadrature formula is manifestly invariant with respect to horizontal translations, as implicit in the travelling wave ansatz. Because of the polynomial dependence on ζ, it is perhaps less obvious that the quadrature is also invariant with respect to vertical translations of the reference frame, as a direct calculation readily shows.

We remark that the quadrature (2.8) is derived without assuming irrotational flow in each layer; a weak $O(\epsilon^2)$ horizontal, y-component, of vorticity is compatible with this expression. However, it is customary in the literature to consider irrotational waves, and we reconstruct the velocity field dependence on z from knowledge of its layer mean (2.3) at this order $O(\epsilon^2)$ under this assumption. This leads to the velocity expressions (cf. Camassa *et al.* 2006)

$$u_k(X,z)=\overline{u}_k+\left(\frac{\eta_k^2}{6}-\frac{(z_k+h_k)^2}{2}\right)(\overline{u}_k)_{XX},\qquad w_k(X,z)=-(\overline{u}_k)_X(z_k+h_k), \tag{2.9}$$

with $z_k=(-1)^k z$, which are asymptotic with errors $O(\epsilon^4)$ and $O(\epsilon^3)$, for the horizontal and vertical velocity, respectively. With these expressions at hand, one can show that the integration constants C_3, C_4 correspond, up to terms of $O(\epsilon^4)$, to the motion invariants for stationary flows given by the Bernoulli constants in each layer

$$R_k=p_k+\frac{\rho_k}{2}(u_k^2+w_k^2)+\rho_k g z,$$

$k=1,2$, and the extended horizontal momentum flux or flow force

$$S=\int_{-h_2}^{h_1}\left(p+\rho u^2\right)\mathrm{d}z.$$

More precisely, these constants are defined by

$$C_3=\mathscr{R}\equiv R_1-R_2,\quad C_4=\mathscr{S}\equiv S-R_2H+\frac{g}{2}(\rho_1 h_1^2-\rho_2 h_2^2),$$

i.e. the Bernoulli differential constant $\mathscr{R}$ and the reduced flow force $\mathscr{S}$, respectively, in the terminology of Bridges & Donaldson (2007). With these definitions, we recover the same quadrature formula as in Miyata (1985).

We note that there appears to be no rigorous proof regarding the minimal set of constants of motion for general symmetric periodic solutions of Euler equations in two-layer systems. Such a proof has been provided in recent years by Benjamin (1995) for the one-layer case, addressing a long-standing conjecture by Benjamin & Lighthill (1954) based on a model of small-amplitude, long-wave periodic motion. Thorpe (1968) presents a similar construction for a two-layer (weakly nonlinear) system; in his approach (as in Miyata 1985), however, five wave-frame invariants generalizing

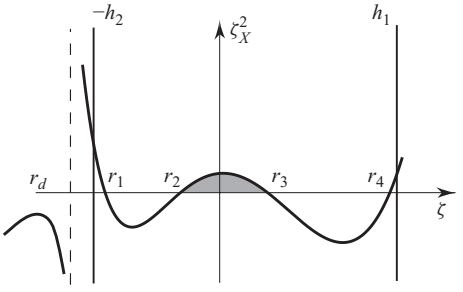

FIGURE 2. Potential for the quadrature (2.8). $r_1, \ldots, r_4$ are the roots of the quartic numerator while r_d is the root of the denominator, always located 'outside' the physical domain.

those in Benjamin & Lighthill (1954) would be needed to completely characterize a periodic wavetrain, viz. mass fluxes in each layer, Bernoulli constants in each layer and total flow force. In fact, the Bernoulli constants, being related by pressure continuity at the interface, are not independent, and only the difference between them ($\mathscr{R}$) can be regarded as a true motion invariant. Moreover, unlike the solitary wave case, in the periodic setting there is no reference state to which an asymptotic pressure head can be related, which allows (one of) the Bernoulli constants to be fixed. Thus, an additional invariant ($\mathscr{S}$ in our notation) needs to be obtained by eliminating the arbitrary Bernoulli constants from the flow force (cf. Bridges & Donaldson 2007).

The quadrature (2.8) corresponds to the classical case of a particle in an unbounded potential well. The potential is a rational function of ζ with a quartic polynomial at the numerator (recall that $\eta_1 = h_1 - \zeta$ and $\eta_2 = h_2 + \zeta$)

$$P(\zeta) = \rho_1 C_1^2 \eta_2 + \rho_2 C_2^2 \eta_1 - \gamma \zeta^2 \eta_1 \eta_2 + 2C_3 \eta_1^2 \eta_2 - 2C_4 \eta_1 \eta_2, \tag{2.10}$$

and a monomial at the denominator, $\rho_1 C_1^2 \eta_2 + \rho_2 C_2^2 \eta_1$. The numerator is positive for large ζ, with $\lim_{\zeta \to \pm\infty} P(\zeta) = +\infty$, while the denominator is always positive inside the physical domain (consequently the corresponding root, r_d say, is outside the physical domain), since $\rho_1 C_1^2 \eta_2 + \rho_2 C_2^2 \eta_1 > 0$. For periodic solutions to exist, there needs to be two roots of the numerator $P(\zeta)$, with $P > 0$ between these roots. Hence, generically, there must be four real roots of the polynomial $P(\zeta)$ to have periodic solutions. These roots can be ordered by magnitude, $r_1 < r_2$ etc., and periodic solutions will vary between the trough position r_2 and the crest position r_3, see figure 2. This structure – five real roots, four for numerator and one for denominator – gives rise to hyperelliptic integrals, in contrast to the elliptic integrals that arise in the solitary wave solutions, which correspond to the limiting situation of root collisions of P.

Unfortunately, manipulations of hyperelliptic integrals have not been completed to a level comparable to their elliptic counterparts. A modicum of information on the solutions of (2.8) can be obtained in terms of the twelve slotted, five variable, Lauricella D multiple hypergeometric function, $F_D^{(5)}$ (see e.g. Drociuk 2004).

We remark that in deriving the quadrature (2.8), we have not used any assumption of symmetry, yet this expression yields only symmetric wave shapes. Thus, we can infer that in the framework of the asymptotic model in Choi & Camassa (1999), long periodic waves are symmetric up to $O(\epsilon^4)$ corrections. We also note that, since the root of the denominator of the quadrature is always outside the physical domain (aside from special limits), singular solutions with cusps (infinite derivative) cannot exist, which is a desirable outcome as such solutions would violate the assumptions underlying the derivation of the long-wave model. Degenerate limits of periodic waves

thus occur only as limits to solitary waves or fronts corresponding to root collisions in the numerator of the quadrature (2.8). The only other degenerate limits correspond to the possibility of vanishing denominator in the quadrature (2.8). This happens when the root of the denominator limits to either $\zeta = h_1$ or $\zeta = -h_2$ (from above or below, respectively), or this root migrates to infinity, which can happen when the coefficient $\rho_2 C_2^2 - \rho_1 C_1^2$ of ζ vanishes. In the former case, the potential becomes cubic, similar to the well-known case of Korteweg–de Vries (KdV) solutions, while in the latter case the potential is a quartic, which is more akin to solutions of the KdV-modified-KdV (or Gardner) equation. We remark that the first degeneracy necessarily occurs when either $C_1 = 0$ or $C_2 = 0$, as well as in the limit of upper fluid density $\rho_1 = 0$. The latter will be discussed below together with the other physically extreme cases in the context of wave profile solutions.

3. Physical interpretation of the integration constants

The results of the previous section show that periodic wave solutions of the long-wave model depend on four parameters that are wave-frame quantities, with the phase speed of the wave not being present in the quadrature (2.8). However, in actual experimental set-ups for the generation of any kind of internal waves, there would be an unambiguously defined laboratory frame of reference. This compels us to consider the phase speed as an additional degree of freedom, and thus to conclude that periodic wave solutions of the long-wave model are a five-parameter family. In general, we can expect some of these five parameters to be fixed by the details of the experimental set-up for an entire family of waves. For instance, in a closed wave tank, one would naturally try to create waves with a wavemaker that achieves various amplitudes and periods, while the mean level of the interface would stay close to that of the quiescent initial state. In addition, a wavemaking mechanism such as the plunger used by Thorpe (1968), which is activated by vertical forces only, may impart zero net horizontal momentum to the fluid. Moreover, incompressibility in a closed tank implies that the total (i.e. across the entire fluid column) volume flux in the lab frame has to be zero. The resulting wave class would thus be constrained to satisfy fixed mean interface (located at $z = 0$, say), zero total horizontal momentum and zero total volume flux. The first two constraints could be assumed to hold locally per period box. These constraints restrict the five-parameter family of periodic waves to a two-parameter family, e.g. amplitude and speed, with the period being functionally dependent on these. Other constraints among the five degrees of freedom are possible, regardless of the physical means of generating periodic waves on a given background state, and have been used in the literature.

With this in mind, in this section, we establish connections between conserved quantities for periodic wave motion and the four constants of integration $C_1, \ldots, C_4$ and the phase speed c present in the quadrature (2.8). We will use the relations developed here primarily to construct various classes of periodic waves in § 4 and Appendix C, as well as to study the properties of these classes. We group these quantities in two categories: properties that are invariant with respect to a Galilean change of reference frame and properties that depend on a particular inertial frame of reference.

3.1. *Other reference frame invariant quantities*

We now specify the functional dependence of other relevant physical quantities, amplitude, period, kinetic and potential energy, and horizontal mean Eulerian velocity,

on the quadrature constants. This is needed to consider all forms of constraints used in the literature for constructing periodic wavetrains.

Let $\boldsymbol{C}$ denote the set of integration constants $\{C_1, C_2, C_3, C_4\}$ and $R(\zeta, \boldsymbol{C})$ denote the rational function in ζ in the right-hand side of the quadrature (2.8), the 'potential well' function. We use script characters to differentiate between physical quantities defined through this quadrature and the values these quantities assume in the range of their functional dependence on $\boldsymbol{C}$, whenever confusion between these two notions can arise. With this notation, the amplitude (defined as distance from peak to trough) is

$$\mathscr{A}(\boldsymbol{C}) = r_3(\boldsymbol{C}) - r_2(\boldsymbol{C}), \tag{3.1}$$

the period is given by the hyperelliptic integral

$$\mathscr{L}(\boldsymbol{C}) = \int_{r_2(\boldsymbol{C})}^{r_3(\boldsymbol{C})} \frac{\mathrm{d}\zeta}{\sqrt{R(\zeta, \boldsymbol{C})}}, \tag{3.2}$$

and the mean position of the interface (cf. Williams 1981 for a discussion) reads

$$\widetilde{\zeta}(\boldsymbol{C}) = \frac{1}{\mathscr{L}(\boldsymbol{C})} \int_{r_2(\boldsymbol{C})}^{r_3(\boldsymbol{C})} \frac{\zeta \,\mathrm{d}\zeta}{\sqrt{R(\zeta, \boldsymbol{C})}}. \tag{3.3}$$

Thus, for instance, the requirement that the mean of the interface coincides with the interface of the background state, which we assume with no loss of generality to be located at the vertical origin of the coordinate system, can be met by imposing the integral constraint $\widetilde{\zeta}(\boldsymbol{C}) = 0$.

Finally, the total potential energy required for deforming the interface from the quiescent state to the wave shape, averaged over the period, is

$$V(\boldsymbol{C}) = \frac{\gamma}{2\mathscr{L}(\boldsymbol{C})} \int_{r_2(\boldsymbol{C})}^{r_3(\boldsymbol{C})} \frac{\zeta^2 \mathrm{d}\zeta}{\sqrt{R(\zeta, \boldsymbol{C})}}. \tag{3.4}$$

3.2. *Frame-dependent quantities*

In the following, we relate volume fluxes, momenta and kinetic energy to the integration constants $\boldsymbol{C}$ and the phase speed and determine how these quantities transform with change of frame of reference. (We remark that in deducing the relations between these quantities and the quadrature constants we do not assume irrotationality of the motion; the formulae we derive can be used in determining classes of long periodic waves under weak rotational approximations consistent with the model.) We denote by $\widehat{\cdot}$ quantities in the wave frame, i.e. the frame where the wave is stationary. Two of the integration constants in the quadrature, C_1 and C_2, have a clear physical interpretation, namely volume fluxes in the wave frame in each layer. Indeed, the volume flux in the wave frame for the layer k is, by virtue of continuity in each layer (2.6),

$$\widehat{Q}_k = \int_{[\eta_k]} (u_k - c)\mathrm{d}z = \overline{u}_k \eta_k - c\eta_k = C_k\,, \quad k = 1, 2. \tag{3.5}$$

We note that these layer volume fluxes are space and time independent solely in the wave frame, and only the total volume flux across any vertical surface is constant in the lab frame. The total volume fluxes in the wave frame and the lab frame are,

respectively,

$$\widehat{Q}(C_1, C_2) = C_1 + C_2, \tag{3.6}$$

$$Q(c, C_1, C_2) = C_1 + C_2 + cH. \tag{3.7}$$

The period-averaged horizontal momentum in layer k (in the lab frame) is given by

$$I_k = \frac{1}{\mathscr{L}(\boldsymbol{C})} \int_{-\mathscr{L}(\boldsymbol{C})/2}^{\mathscr{L}(\boldsymbol{C})/2} \int_{[\eta_k]} \rho_k u_k \, \mathrm{d}z \, \mathrm{d}X = \frac{1}{\mathscr{L}(\boldsymbol{C})} \int_{-\mathscr{L}(\boldsymbol{C})/2}^{\mathscr{L}(\boldsymbol{C})/2} \rho_k \eta_k \overline{u}_k \, \mathrm{d}X, \quad k = 1, 2. \tag{3.8}$$

Integrating (2.6) over the period after multiplication with ρ_k yields

$$I_k - c\rho_k \widetilde{h}_k = \rho_k \widehat{Q}_k, \quad k = 1, 2,$$

where $\widetilde{h}_k$ denotes the period-average of η_k. Thus, the period-averaged horizontal momenta for layer k in the wave frame and the lab frame, respectively, are

$$\widehat{I}_k(C_k) = \rho_k C_k, \tag{3.9}$$

$$I_k(c, \boldsymbol{C}) = \rho_k C_k + c\rho_k \widetilde{h}_k(\boldsymbol{C}), \quad k = 1, 2, \tag{3.10}$$

so that the period-averaged total horizontal momenta in the wave and lab frames are

$$\widehat{I}(C_1, C_2) = \rho_1 C_1 + \rho_2 C_2, \tag{3.11}$$

$$I(c, \boldsymbol{C}) = \rho_1 C_1 + \rho_2 C_2 + c(\rho_1 \widetilde{h}_1(\boldsymbol{C}) + \rho_2 \widetilde{h}_2(\boldsymbol{C})), \tag{3.12}$$

respectively. We remark that the above quantities are exact conservation laws for two-layer Euler equations which derive simply from conservation of mass (and volume, by incompressibility). As such, they also hold exactly for the model, since mass is conserved with no asymptotic errors (cf. (2.1)). We further remark that, in general, for two-layer Euler periodic solutions even when expressed by a multiply-valued interface function (such as the case of 'overhanging' waves in § 6), incompressibility implies that the total volume flux is

$$Q = \frac{I_1}{\rho_1} + \frac{I_2}{\rho_2}, \tag{3.13}$$

which, together with the total period-averaged horizontal momentum $I = I_1 + I_2$, provides a one-to-one correspondence between constraints applied to total fluid domain-defined quantities I, Q and layer-defined quantities I_1, I_2. In particular, this implies that when these total quantities are chosen to be zero, so are the layer momenta I_1 and I_2 and vice versa.

Next, we express the kinetic energy per period in terms of the quadrature constants and the phase speed. The period-averaged kinetic energy for layer k is given by

$$T_k = \frac{\rho_k}{2\mathscr{L}(\boldsymbol{C})} \int_{-\mathscr{L}(\boldsymbol{C})/2}^{\mathscr{L}(\boldsymbol{C})/2} \int_{[\eta_k]} (u_k^2 + w_k^2) \, \mathrm{d}z \, \mathrm{d}X, \tag{3.14}$$

with u and w denoting the horizontal and vertical velocity components. We use the asymptotic relations (2.9) for these components; carrying out the integration across the layer in (3.14) yields

$$T_k = \frac{\rho_k}{2\mathscr{L}(\boldsymbol{C})} \int_{-\mathscr{L}(\boldsymbol{C})/2}^{\mathscr{L}(\boldsymbol{C})/2} \left[\overline{u}_k^2 \eta_k + (\overline{u}_k)_X^2 \frac{\eta_k^3}{3} \right] \mathrm{d}X, \tag{3.15}$$

which, by using (3.5), (3.10) and the asymptotic relation for velocity (2.9), can be put in the form

$$T_k = \frac{\rho_k C_k}{2}\frac{1}{\mathscr{L}(\boldsymbol{C})}\int_{-\mathscr{L}(\boldsymbol{C})/2}^{\mathscr{L}(\boldsymbol{C})/2} u_k(X,(-1)^k h_k)\mathrm{d}X + \frac{cI_k}{2}, \quad k=1,2. \tag{3.16}$$

We recognize in the first term of the above relation the mean Eulerian (horizontal) velocity for layer k, defined as $\widetilde{u}_k = (1/L)\int_{-\mathscr{L}/2}^{\mathscr{L}/2} u_k(X,z)dX$, where z is any location within the layer k that does not intersect the interface. This integral quantity can be shown to be independent of z (within the assumed range) and can be expressed in terms of the constants of integration $\boldsymbol{C}$ by using the asymptotic relation for velocity (2.9)

$$\widetilde{u}_k(c,\boldsymbol{C}) = c + \frac{1}{\mathscr{L}(\boldsymbol{C})}\int_{r_2(\boldsymbol{C})}^{r_3(\boldsymbol{C})} \frac{C_k\,(3+R(\zeta,\boldsymbol{C}))}{3\eta_k\sqrt{R(\zeta,\boldsymbol{C})}}\mathrm{d}\zeta, \tag{3.17}$$

neglecting terms of order $O(\epsilon^4)$.

Hence, the kinetic energy in the layer k in terms of the quadrature constants and the phase speed is

$$T_k(c,\boldsymbol{C}) = \frac{\rho_k \widehat{Q}_k \widetilde{u}_k}{2} + \frac{cI_k}{2}, \tag{3.18}$$

where $\widehat{Q}_k$, the volume flux in the wave frame in the layer k, is given by (3.5), $\widetilde{u}_k$, the mean Eulerian velocity in layer k, is given by (3.17) and I_k, the horizontal momentum in the lab frame for the layer k, is given by (3.10). We remark that the expression of the kinetic energy (3.18), being derived from an asymptotic approximation to the velocity field, is in principle affected by the accuracy of the asymptotic model. However, with this equation we retrieve the exact form deduced by Klopman (1990) for irrotational periodic wave trains in one-layer fluids, building upon previous work by Longuet-Higgins (1975), who assumed that the lab frame was defined as the frame for which the mean Eulerian velocity is zero.

4. Constrained solution class: zero total volume flux and horizontal momentum periodic waves

We proceed with constructing the class of periodic waves we have alluded to in the previous section, satisfying three constraints: fixed mean level of the interface, total horizontal momentum in the lab frame zero and total volume flux in the lab frame zero. These constraints leave two free parameters. For our purposes, we found that the most advantageous choice to solve the system and describe solution properties is to parametrize the family with amplitude A and phase speed c. We will first describe how to determine particular solutions for prescribed amplitude and speed. We will then determine the domain of existence of periodic wave solutions in the parameter space $(A\,,c)$ and study their limiting forms.

4.1. *Periodic solutions for prescribed speed and amplitude*

By requiring that the total volume flux given by (3.7) and total horizontal momentum per period given by (3.12) are zero, the resulting linear system relates the two constants of integration in the quadrature C_1 and C_2 to the phase speed and mean heights

$$C_k = -c\widetilde{h}_k, \qquad k=1,2. \tag{4.1}$$

Note that it then follows from (3.10) that the period-averaged horizontal momentum in each layer is zero. By choosing the coordinate system at the level of the quiescent state,

the constraint of zero mean displacement of the interface implies $\widetilde{h}_k = h_k, k = 1, 2$. The constants C_3 and C_4 can be determined by seeking waves of amplitude A and imposing the constraint of zero mean of interface displacement

$$\mathscr{A}(c, C_3, C_4) = A, \quad \widetilde{\zeta}(c, C_3, C_4) = 0. \tag{4.2}$$

We first relate the two remaining constants of integration C_3 and C_4 to the position of the crest and the position of the trough, which are given by the middle roots of the quartic polynomial from the numerator of (2.8). If α is the position of the crest (so $\alpha - A$ is the position of the trough) C_3 and C_4 are functions of α since α and $\alpha - A$ must be roots of the polynomial $P(\zeta)$. By imposing this condition and solving the resulting linear system, we have

$$C_3(\alpha) = \frac{c^2\rho_1 h_1^2}{2(h_1 - \alpha)(h_1 - \alpha + A)} - \frac{c^2\rho_2 h_2^2}{2(h_2 + \alpha)(h_2 + \alpha - A)} - \gamma\left(\alpha - \frac{A}{2}\right), \tag{4.3}$$

$$C_4(\alpha) = C_3(\alpha)(A + h_1 - \alpha) + \frac{c^2\rho_1 h_1^2}{2(A + h_1 - \alpha)} - \frac{c^2\rho_2 h_2^2}{2(A - h_2 - \alpha)} - \frac{\gamma}{2}(A - \alpha)^2. \tag{4.4}$$

With the explicit expressions for all the coefficients thus determined, the other two roots of the quartic $P(\zeta)$ can in turn be determined in terms of explicit (albeit lengthy) algebraic functions of α and A by solving the quadratic polynomial that results from factoring the roots α and $\alpha - A$. Similarly, the mean of the interface becomes a function of α through (4.3), (4.4) in (3.3) (suppressing for ease of notation the arguments C_1 and C_2 of the rational function R in the quadrature expression (2.8))

$$\widetilde{\zeta}(\alpha) = \int_{\alpha - A}^{\alpha} \frac{\zeta\,\mathrm{d}\zeta}{\sqrt{R(\zeta, C_3(\alpha), C_4(\alpha))}} \Bigg/ \int_{\alpha - A}^{\alpha} \frac{\mathrm{d}\zeta}{\sqrt{R(\zeta, C_3(\alpha), C_4(\alpha))}}. \tag{4.5}$$

Hence, the position of the crest of the periodic solution can be determined by finding the root of the nonlinear equation

$$\widetilde{\zeta}(\alpha) = 0. \tag{4.6}$$

Note that the denominator in (4.5) is a positive quantity, hence a necessary condition for existence of a solution is for the integrand of the function in the numerator

$$f(\alpha) \equiv \int_{\alpha - A}^{\alpha} \frac{\zeta}{\sqrt{R(\zeta, C_3(\alpha), C_4(\alpha))}}\mathrm{d}\zeta \tag{4.7}$$

to change sign in the interval $(\alpha - A, \alpha)$, which implies $\alpha - A < 0 < \alpha$. This leads to a criterion for the existence of a solution satisfying all the requirements so far imposed, by seeking the two limiting positions for the crest α when two roots of the polynomial (2.10) collide. Let

$$\alpha_{min}(A, c) \equiv \alpha(A, c)|_{r_1(\alpha;A,c)=r_2(\alpha;A,c)} \tag{4.8}$$

and

$$\alpha_{max}(A, c) \equiv \alpha(A, c)|_{r_3(\alpha;A,c)=r_4(\alpha;A,c)} \tag{4.9}$$

denote the α-range lower and upper limits, respectively, where the polynomial (2.10) has double roots $\beta_e(A, c) = r_1 = r_2 = \alpha_{min}(A, c) - A$ and $\beta_d(A, c) = r_3 = r_4 = \alpha_{max}(A, c)$. Note that these would correspond to amplitude-A solitary waves of, respectively, elevation and depression. Note also that these are not limiting forms of the class of periodic waves that satisfy our requirements. Thus, the

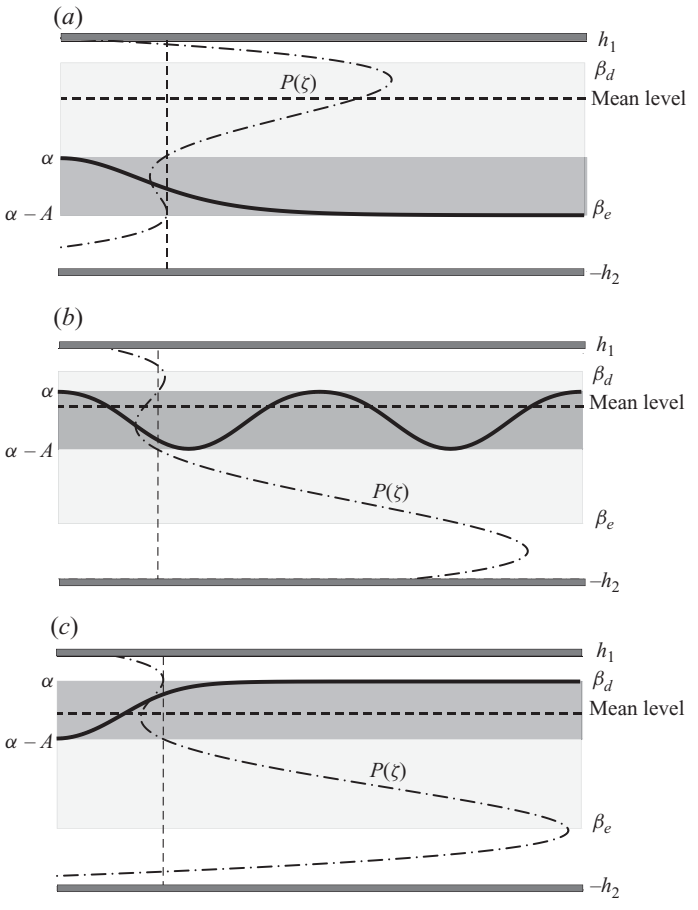

FIGURE 3. Schematic construction of constrained solutions with zero momenta and mean elevation for given amplitude A and speed c. The fluid is confined between the top and bottom walls at $z = h_1$ and $z = -h_2$, respectively. The dark grey strip 'highlights' the range of the interface function $\zeta(X)$ between the roots at α and $\alpha - A$, while the light grey strip identifies the allowable range determined by root coalescence at $\alpha - A = \beta_e(A, c)$ and $\alpha = \beta_d(A, c)$, corresponding to solitary waves of elevation and depression, respectively. Solid curves depict travelling wave solution profiles (only the right half for solitary waves). The location of the targeted mean level is marked by the dashed horizontal line and the quartic function $P(\zeta)$, shown by the dash-dotted curve, varies according to the placement of α in the allowable range from (*a*) to (*c*); (*a*) $\alpha = \beta_e(A, c) + A$, (*b*) $\beta_e(A, c) < \alpha < \beta_d(A, c)$ and (*c*) $\alpha = \beta_d(A, c)$. This construction is based on the actual configuration given by $h_1/h_2 = 1/3$, $\rho_1/\rho_2 = 0.99$, $c/c_0 = 0.55$, $A/h_1 = 1$.

necessary condition for existence of a periodic solution becomes

$$\beta_e(A, c) < 0 < \beta_d(A, c); \tag{4.10}$$

see figure 3 for an illustration of the connection between the position of the crest α and the roots in such an instance. Moreover, as $\alpha \to \alpha_{min}(A, c)$, $f(\alpha) \to -\infty$, whereas as $\alpha \to \alpha_{max}(A, c)$, $f(\alpha) \to \infty$. It follows that $f(\alpha)$ will have a zero for some α in the range $(\alpha_{min}, \alpha_{max})$, so that the condition $\beta_e(A, c) < 0 < \beta_d(A, c)$ is also sufficient for the existence of a periodic solution of mean zero. We remark that this argument

does not guarantee uniqueness of zeros of $f(\alpha)$ and hence of periodic solutions of mean zero. This would be guaranteed by the monotonicity of either $\widetilde{\zeta}(\alpha)$ or the function $f(\alpha)$. Numerical results confirm that both these functions are monotonic in the interval $(\alpha_{min}, \alpha_{max})$, but a rigorous proof is still lacking.

4.2. *Domain of existence*

The considerations of the previous section allow us to outline a strategy for determining periodic wave solutions of prescribed amplitude and speed, namely, given an A and a c, we can check whether the double roots $\beta_e(A, c)$ and $\beta_d(A, c)$ have opposite sign, which implies the existence of the periodic train of that amplitude and speed satisfying the constraints of zero mean displacement, zero period-averaged horizontal momentum and zero period-averaged volume flux. Of course, actual construction of the periodic train would have to rely on a numerical root-finding algorithm. Hence, it would be desirable to know *a priori* and to determine analytically the portion of the (A, c) quadrant where the sufficiency condition (4.10) holds.

To this end, we use the two families of solitary wave solutions of elevation and depression corresponding to $\beta_e(A, c)$ and $\beta_d(A, c)$, respectively. In fact, the limiting forms β_d and β_e are nothing else than a generalization of the solitary waves (or fronts) solutions derived in Choi & Camassa (1999), which admit an explicit analytical representation. In particular, the amplitude–speed relations of these families foliate the (A, c) quadrant and their limiting front solutions provide a boundary of existence in this quadrant, with the amplitude–speed relation given by an explicit quadratic expression. Note that the quadrature is invariant with the change of the position of the coordinate system in the vertical direction. Hence, we can represent the family of solitary waves corresponding to the double roots $\beta_e(A, c)$ and $\beta_d(A, c)$, with a new parametrization (β, c), with respect to 'artificial' height configuration $h_1 - \beta, h_2 + \beta$ for $\beta \in (-h_2, h_1)$. The advantage of this new parametrization is that the polynomial at the numerator of the quadrature can be expressed as a product of ζ^2 times a quadratic polynomial, which provides the amplitude in closed form; see Choi & Camassa (1999). These 'foliating' solitary wave solutions would then span a domain in the parameter space (β, c), and this domain can in turn be mapped easily in the parameter space (A, c). Note that in order to be useful for the construction of the periodic wavetrain that satisfies our constraints, these solitary waves of elevation and depression corresponding to double root β_e and β_d in the polynomial (2.10) must satisfy condition (4.1), and hence they have prescribed volume fluxes in the wave frame. By imposing the boundary conditions at infinity, we obtain

$$(\overline{u}_k|_\infty - c)\eta_k|_\infty = -ch_k, \qquad k = 1, 2, \tag{4.11}$$

where $\overline{u}_k|_\infty$ can be interpreted as a current at infinity for the layer k in the lab frame while $\eta_k|_\infty$ is the height of layer k at infinity, since $\eta_k|_\infty \neq h_k$. Thus, these foliating solitary wave solutions are generalizations of the standard solitary waves in Choi & Camassa (1999), for which the background state has zero currents in the lab frame. In Appendix A, we present an overview of this more general class of solitary waves, which are of independent interest than the present focus on periodic waves.

The domain of existence in (β, c) of solitary waves with the prescribed fluxes (4.11) can be found by fixing β and determining the range of speed c for which solitary waves with property (4.11) exist. In Appendix B, we present details for determining this range. For fixed β, the dependence between the maximum interface

displacement a (or signed amplitude, defined as difference between the zero level in the 'artificial' parameters and the peak of the wave) and speed c is given by (B 9) for $c \in [c_{min}(\beta)\,, c_f(\beta)]$, where $c_{min}(\beta)$ and $c_f(\beta)$ correspond to limiting speeds of solitary wave of zero amplitude and front given by (B 5) and (B 6), respectively, and $z = \beta_0$ is a constant level in the physical domain $z \in [-h_2, h_1]$ determined solely by the 'hardware' parameters h_k, ρ_k, $k = 1, 2$; see definition (B 8).

For fixed β, the sign of the maximum displacement $a(c\,;\beta)$ shows the polarity of the class of solitary waves, with $a(c\,;\beta) > 0$ corresponding to waves of elevation, and $a(c\,;\beta) < 0$ to depression, respectively, for all $c \in \big[c_{min}(\beta), c_f(\beta)\big]$. In Appendix B, we show that if $\beta < \beta_0$, then the corresponding maximum displacement branch $a(c\,;\beta)$ is positive (elevation), and, conversely, if $\beta > \beta_0$ then $a(c\,;\beta) < 0$ (depression). Thus, we can infer that the curves $a(c\,;\beta)$ with $\beta < \beta_0$ correspond to the foliating family β_e, whereas the curves $a(c\,;\beta)$ with $\beta > \beta_0$ correspond to the foliating family β_d. These families span a domain in the (a, c)-semi-plane $c > 0$, bounded by a curve represented parametrically by

$$a\left(c_f(\beta)\,;\beta\right), c_f(\beta), \qquad \beta \in (-h_2, h_1),$$

which corresponds to front solutions. By eliminating β, we can obtain an explicit formula for the front branch corresponding to $a\left(c_f(\beta)\right)$, with $\beta \in (-h_2, h_1)$. Let $h_r \equiv h_1/h_2$ and $\rho_r \equiv \rho_1/\rho_2$. When $h_r\sqrt{\rho_r} \neq 1$, the front branch is given by relation (B 11), whereas for $h_r\sqrt{\rho_r} = 1$ by relation (B 14). We remark that this particular depth ratio, which is different from the critical depth ratio $h_r = \sqrt{\rho_r}$, is associated with a mathematical degeneracy of the quadrature formula (2.8) to elliptic functions, a situation that does not seem to have any particular physical interpretation.

The curve $c_f(a)$ is symmetrical with respect to c axis. Returning to the original parameters A, c, for which $A > 0$, corresponds to 'folding' the left half of the symmetric domain in the a, c plane on top of the right half (see figure 4), by taking $A = |a|$. Thus, for any point in the quadrant (A, c) with $c \in [0, c_f(A)]$ and $A \in [0, H]$, there are two foliating solitary waves of opposite polarity. These waves define a window for the possible locations of the crest and trough of a periodic wave of amplitude A that satisfies the flux condition (4.1). Moreover, the zero mean of the interface condition necessarily requires the crest location to be positive while the trough location must be negative, according to (4.10). This condition selects a limiting foliating curve

$$A(c;0) = |a(c;0)|, \qquad c \in \left[c_{min}(0), c_f(0)\right], \tag{4.12}$$

when $\beta = 0$, which further restricts the allowable domain in the A, c plane. (For the region above this curve, the two β parameters corresponding to the two families of foliating solitary waves have the same sign.) Note that the curve $a(c;0)$ with $c \in [c_0, c_m]$ corresponds to the standard solitary waves asymptotic to layer thicknesses h_1, h_2. In the above, c_0 is the long-wave critical speed for this configuration

$$c_0^2 = \frac{(1-\rho_r)h_r}{(\rho_r + h_r)(h_r + 1)} gH, \tag{4.13}$$

while c_m, the speed of the highest travelling waves in Choi & Camassa (1999), and the corresponding maximum amplitude $a_m(c_m\,;0)$ are given by

$$c_m^2 = \frac{1-\sqrt{\rho_r}}{1+\sqrt{\rho_r}} gH, \quad a_m = \frac{h_r - \sqrt{\rho_r}}{(h_r+1)(\sqrt{\rho_r}+1)} H. \tag{4.14}$$

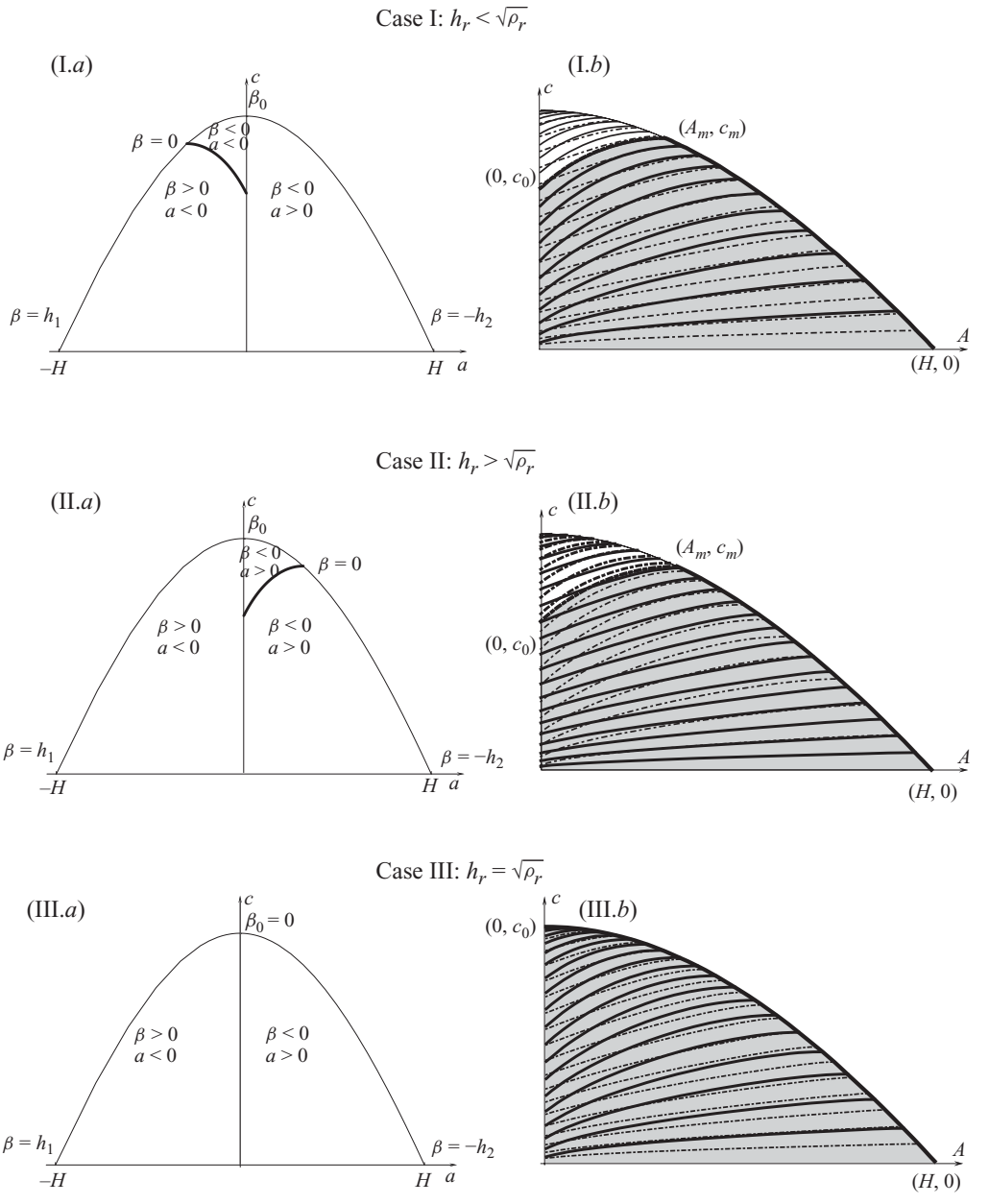

FIGURE 4. (I.*a*), (II.*a*) and (III.*a*) The front branch that marks the domain of existence of foliating solitary waves. (I.*b*), (II.*b*) and (III.*b*) Domain of existence for periodic waves of zero horizontal momentum and zero flux (grey areas). The thicker curves correspond to foliating solitary waves with $\beta > 0$ whereas thinner curves correspond to $\beta < 0$; continuous curves correspond to foliating solitary waves of depression, dashed curves to elevation. Periodic solutions can exist only in domains covered by solitary wave curves with opposite polarities and opposite positions of the interface at infinity.

Hence, the curve $A(c;0)$ corresponds to the infinite period limit to solitary waves of the periodic waves in our class, i.e. total horizontal momentum zero, total volume flux zero and zero mean elevation. Indeed, these limiting solitary waves satisfy the mean zero of the interface condition in the limit, because in the process of taking the

mean the finite mass is divided by an infinite period. We can represent this branch of the boundary as a function of amplitude A, by inverting (4.12)

$$c_{sw}(A) = c_0\sqrt{\frac{(h_1 - \mathrm{sgn}(\beta_0)A)(h_2 + \mathrm{sgn}(\beta_0)A)}{h_1h_2 - \left(c_0^2/g\right)\mathrm{sgn}(\beta_0)A}}, \qquad A \in [0,\, A_m] \tag{4.15}$$

with $A_m = |a_m|$ and β_0 given by (B 8). The other boundary of the existence domain $A \in \left[|a_m|\,, H\right] \equiv [A_m, H]$, being the front limit of each foliating solitary wave curve, would correspond to the limit of our periodic waves to fronts.

Therefore, when the speed c increases with A fixed, $A \in [0, A_m]$, the periodic waves limit to infinite period in the form of solitary waves. Conversely, when c increases with $A \in [A_m, H]$, the periodic waves broaden up to fronts. The standard front limit of solitary waves (Choi & Camassa 1999) corresponds to the single point (A_m, c_m) at the vertex of the domain. Apart from this point, the front branch $[A_m, H]$ represents a new class of front solutions. Note that for fixed $c \in [c_0, c_m]$ the domain of existence of periodic waves in our class consists of waves whose amplitude is larger than solitary waves of the same speed, and moreover a portion of the domain of existence consists of periodic waves of amplitude bigger than the maximum amplitude of the solitary wave (which limits to a front) for the same configuration.

We sketch the above discussion in figure 4, for all three relevant cases: (I) $h_r < \sqrt{\rho_r}$, in which the solitary waves limiting branch corresponds to waves of depression; (II) $h_r > \sqrt{\rho_r}$, in which the limiting solitary waves are of elevation; (III) $h_r = \sqrt{\rho_r}$ – the critical density ratio – in which the solitary waves branch vanishes and the boundary of the domain of existence is marked only by the front branch.

We remark, as shown in Appendix A, that the branch of front solutions that forms the right boundary of the existence domain is in fact exact for the parent two-layer Euler system, even though we arrive at it from within the asymptotic model. This property provides a validation test for the numerical solutions of two-layer Euler equations with large periods. We also remark that the vertical and horizontal boundaries of the domain of existence correspond to infinitesimal amplitude waves, and to the singular limit of infinitesimal wave speed where the vanishing period shows that a neighbourhood of the $c = 0$ axis is clearly outside of the model's validity regime. In fact, as we will see in the next section and should be intuitive now given that the wave amplitude spans the whole gap between plates, the point $(H, 0)$ is extremely singular, and in its neighbourhood wavetrains of any period can be found.

4.3. *Extreme density limits*

To complete this section, it is worth pointing out the limiting cases of equal density layers and that of vanishing upper layer density. For the first case, $\rho_r = 1$, the physics clearly cannot support internal wave motion, and this is reflected in the model by the fact that the boundary of the domain of existence collapses to zero, as the equation for the maximum speed (4.14) shows. For the second case, $\rho_r = 0$, which occurs for $\rho_1 = 0$ for a stably stratified fluid, the momentum equation governing the lower layer (2.2) decouples from that of the first layer, thus reducing the system to the single-layer version (Su & Gardner 1969; Green & Naghdi 1976). The effect of this limit on the quadrature (2.8) is to make the potential a cubic since the root at the denominator and a root of the quartic in the numerator collide at the upper boundary of the physical domain h_1. In the limit $\rho_r \to 0$, the family of foliating solitary waves of depression β_d vanishes and the right boundary of the domain of existence consisting of fronts degenerates to a branch of solitary waves that 'scrape' the top wall with

their crests. The left/top boundary consisting of solitary waves when $\rho_1 \neq 0$ remains a branch of solitary waves in the limit $\rho_r \to 0$ and coincides with the 'classic' solitary wave solutions for the strongly nonlinear single-layer model (Su & Gardner 1969; Green & Naghdi 1976).

Curiously, the existence of maximum amplitude value A_m for $\rho_1 \neq 0$, which corresponds to the intersection of the two boundary branches for the existence domain, retains a meaning in the single-layer case as the maximum amplitude of the solitary wave that would fit within the domain walls at $z = -h_2$ and $z = h_1$. This apparent maximum amplitude contrasts the well-known result that, for the single-layer case, the strongly nonlinear model solitary-wave solutions do not possess a limiting amplitude, just as for the weakly nonlinear models such as KdV. Also, we remark that the degenerate front branch consists entirely of 'scraping' solitary waves, and that these could still be thought of as fronts by cutting off half of the wave at the crest (at $z = h_1$). Also note that for this degenerate front branch, the dependence of the speed on amplitude becomes linear.

5. Properties of constrained periodic wave trains

Having determined the domain of existence in the A, c quadrant of our two-parameter family of periodic waves, we now turn to the study of the dependence of other relevant physical properties on these parameters.

5.1. *Wave shapes*

Determining a periodic wave solution for given amplitude and speed is a root-finding problem (4.6) which involves evaluation of a hyperelliptic integral, see (4.5). We use a Newton scheme, whose quadratic convergence is desirable depending on a good initial guess (away from singularities injected into the integral by double roots). Here again the family of foliating solitary waves on artificial parameters becomes useful in identifying the position of the singularities.

Away from the critical depth ratio, when $h_r \neq \sqrt{\rho_r} \equiv h_{critical}$, the maximum amplitude A_m of the solitary wave branch marks a threshold amplitude that separates two regimes $A < A_m$ or $A > A_m$. The properties of the periodic solutions in these two cases are distinctively different.

To fix ideas, let us focus on the case $h_r < h_{critical}$. For fixed amplitude $A < A_m$, as the phase speed increases, the position of the trough approaches the position of the foliating solitary wave of depression β_d while the distance between the trough and the other double root β_e remains bounded away from zero and set by the maximum speed for the corresponding solitary wave limiting form of the same amplitude.

For fixed amplitude $A > A_m$, with increasing phase speed the position of the crest once again approaches β_d, but the trough now also approaches the other double root β_e. However, we remark that for the configuration we are focusing on, $h_r < h_{critical}$, the approach of the trough position to this double root β_e occurs at a much slower rate than the approach of the crest to the other double root β_d.

For the other configuration $h_r > h_{critical}$ this happens in reverse. We illustrate these observations in figure 5 for a configuration with $h_r < h_{critical}$ and in figure 6 for $h_r > h_{critical}$, respectively.

For a configuration corresponding to the critical depth ratio $h_r = \sqrt{\rho_r}$, when the boundary of the domain of existence consists only of fronts, the position of the crest approaches the limiting position β_d at a slightly faster rate than the position of the trough approaches β_e; see figure 7.

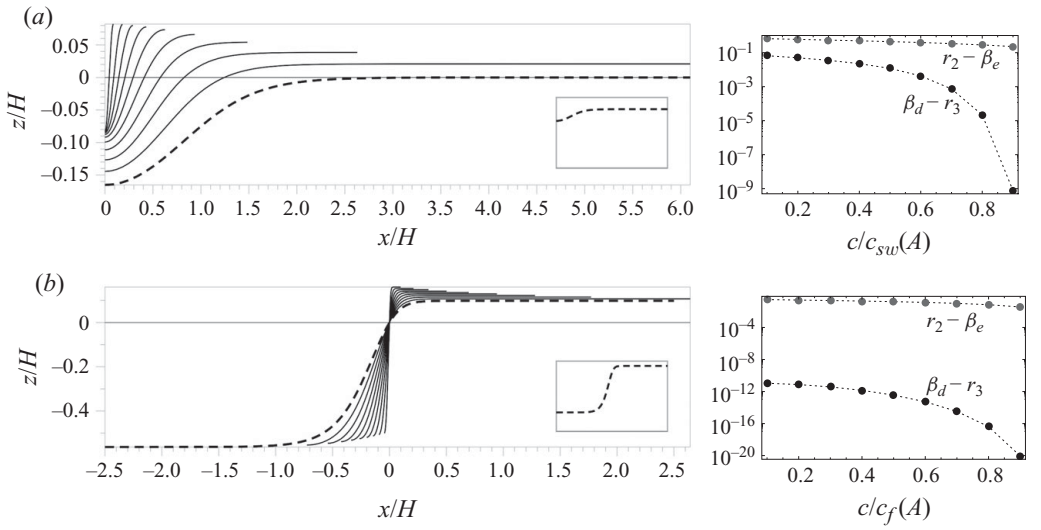

FIGURE 5. Wave profiles (half a period) along with the corresponding distances between the crest and the double root β_d and the trough and the double root β_e, respectively, for a configuration with $h_r < \sqrt{\rho_r}$ ($h_1/H = 1/6$, $h_2/H = 5/6$ and $\rho_r = 0.97$), for fixed amplitude (*a*) $A = A_m/2$ and (*b*) $A = 2A_m$ and phase speeds ranging from 10 % to 90 % of the corresponding maximum speed (*a*) $c_{sw}(A)$ and (*b*) $c_f(A)$, respectively. The dashed profiles correspond to the limiting (*a*) solitary wave of amplitude $A = A_m/2$ and (*b*) front of amplitude $A = 2A_m$; they are also depicted in the insets where the physical boundaries $-h_2$, h_1 are included.

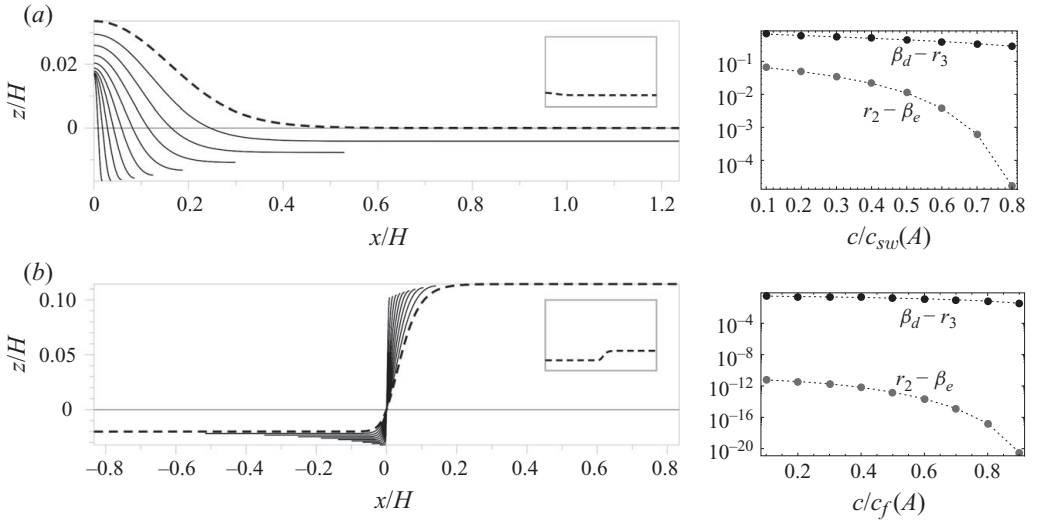

FIGURE 6. Same as in figure 5 for a configuration with $h_r > \sqrt{\rho_r}$ ($h_1/H = 1/1.2$, $h_2/H = 0.2/1.2$ and $\rho_r = 0.97$).

We note that for large amplitudes, even when the pair speed/amplitude is away from the boundary of the domain of existence, the hyperelliptic integrals involved in the root-finding process become nearly singular and consequently high-precision computations are necessary. We remark that the root finding in this situation could be handled analytically via an asymptotic expansion in a small parameter representing

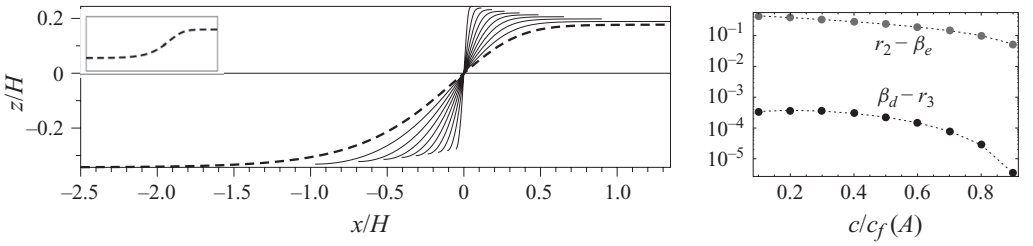

FIGURE 7. Same as in figure 5(*b*) for a configuration corresponding to the critical case $h_r = \sqrt{\rho_r}$ ($h_1/H \simeq 0.24$, $h_2/H \simeq 0.76$ and $\rho_r = 0.1$). The waves have fixed amplitude $A = H/2$ and phase speeds ranging from 10 % to 90 % of the corresponding maximum speed $c_f(H/2)$.

the distance between roots approaching the double root locations β_d or β_e. This analysis, however, involves some subtleties that will be presented elsewhere.

5.2. *Period dependence on speed and amplitude*

Period average expressions such as the kinetic energy depend, of course, on knowing the length L of the period where the average is computed. This is determined through the quadrature by (3.2), and is therefore linked to the process of root finding for our class of solutions described above. Unfortunately, this prevents us from writing a simple and explicit functional dependence of period on A and c, and to find the level sets of L over the (A, c) domain we have to resort to numerical methods. To implement this, we determine the periodic wave solutions at the nodes of a grid covering the existence domain, then compute the corresponding period and construct the level sets by interpolation. Note that for determining the periodic solutions at each node, we need the two limiting positions $\beta_e(A, c)$ and $\beta_d(A, c)$. This requires inversion of the function $a(c; \beta)$ given by (B 9), and the inversion can only be achieved numerically by solving the two equations $a(c; \beta) = A$ and $a(c; \beta) = -A$.

A strategy for reducing the computational cost is to cover the domain of existence with only one of the foliating family of solitary waves, β_d when $h_r < h_{critical}$ or β_e when $h_r > h_{critical}$, by taking into account the observations made in § 5.1. These curves are given in closed form by (B 9) and provide a good initial guess for the position of the crest of periodic waves solutions. For constructing a constant period contour, we (i) determine solutions along the foliating solitary wave curves, by using parameter continuation techniques for accelerating the root-finding process; (ii) interpolate the period as a function of speed c on these curves; (iii) determine for each curve the root c corresponding to that particular period; finally (iv) perform a spline interpolation for the (A, c) pairs found in the previous step.

In figure 8(*a–c*) we present period isolines for two particular configurations corresponding to $h_r < h_{critical}$ and $h_r = h_{critical}$, respectively. There are several interesting qualitative observations that can be made based on these numerical results. First, note that the period increases with the increase of phase speed, which is in agreement with a general result for periodic waves in arbitrary stratification, proved by Yih (1959). Second, all period isolines wrap along the front line as the amplitude increases, converging to a singular limit that corresponds to a steep front of amplitude equal to the total depth of the fluid. Although this limit is mathematically attainable, it is not of practical relevance since it lies outside of the domain of expected validity of solutions with respect to the parent Euler system, as we are going to see in the following section. Third, we note that away from critical depth ratio, we can identify two types of isolines: those along which the phase speeds are subcritical and those

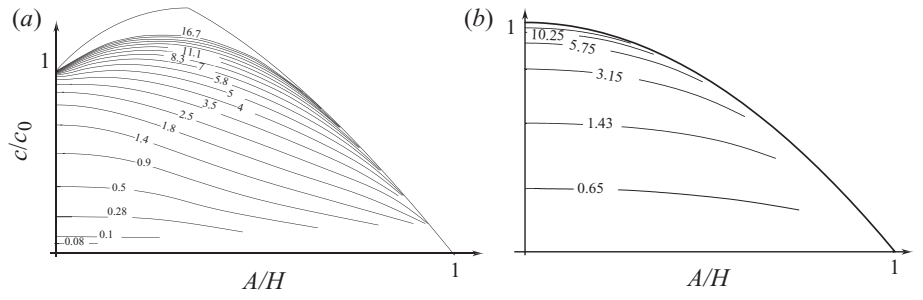

FIGURE 8. Level sets of the period (non-dimensionalized with the total height H) for a configuration with (*a*) $h_r < \sqrt{\rho_r}$ ($h_1/H = 1/6$, $h_2/H = 5/6$ and $\rho_r = 0.97$), (*b*) $h_r = \sqrt{\rho_r}$ ($h_1/H \simeq 0.41$, $h_2/H \simeq 0.58$ and $\rho_r = 0.5$). The case $h_r > \sqrt{\rho_r}$ ($h_1/H \simeq 0.56$, $h_2/H \simeq 0.44$ and $\rho_r = 0.5$) (not shown here) is similar to (*a*).

that contain regions with supercritical speeds. On both sub- and supercritical isolines, the periodic solutions approach one of the two limiting foliating families (β_d for $h_r < h_{critical}$ or β_e for $h_r > h_{critical}$) at a much faster rate than the other as the amplitude increases. However, on subcritical isolines, we can identify a region where both the position of the crest and the trough are nearly symmetrical with respect to the (zero mean) z-axis, and lie away from the bounds given by β_d and β_e. In these regions, the phase speed is comparable with the speed of waves of infinitesimal amplitude.

Finally, we mention that a good approximation to the actual location of the bounding roots α (for waves of depression) or $\alpha - A$ (for waves of elevation), respectively, for fixed amplitude A and period L can be found for sufficiently large period waves by a simple area criterion based on the effective wavelength λ_I (as defined by Koop & Butler 1981 through the area integral of solitary wave profiles) of limiting foliating solutions, based on the closeness result mentioned above.

5.3. *Kinetic and potential energy*

Once the quadrature solution is found, simple expressions for kinetic and potential energy can be derived for the periodic wavetrain, which allows us to examine how equipartition between these two forms of energy is lost as amplitude increases. By using the fact that for our class of periodic waves the horizontal momentum I_k in both layers $k = 1, 2$ is zero, the layer kinetic energy (3.18) in terms of the mean Eulerian velocity (3.17) is

$$T_k = -\frac{\rho_k}{2} c h_k \widetilde{u}_k. \tag{5.1}$$

This expression (which is exact for Euler equations) shows that the mean Eulerian velocity must be negative for periodic waves with zero horizontal momenta in both layers. Notice that the model expression for the kinetic energy (3.18) does not immediately show this property of sign definiteness. However, by replacing the integration constant C_k given by (4.1) in the asymptotic relation (3.17), the mean Eulerian velocity in the layer k can be expressed as a sum of two integrals

$$\widetilde{u}_k = \frac{c}{L} \int_{-L/2}^{L/2} \left[1 - \frac{h_k}{\eta_k}\right] \, \mathrm{d}x - \frac{c}{L} \int_{-L/2}^{L/2} \frac{h_k \zeta_X^2}{3\eta_k} \, \mathrm{d}X, \tag{5.2}$$

with the second being manifestly negative definite. For the first integral, by using Cauchy–Schwartz inequality, we obtain

$$\left(\int_{-L/2}^{L/2}\sqrt{\eta_k}\frac{1}{\sqrt{\eta_k}}\mathrm{d}X\right)^2 \leqslant \int_{-L/2}^{L/2}\eta_k\mathrm{d}X\int_{-L/2}^{L/2}\frac{1}{\eta_k}\mathrm{d}X = h_k L\int_{-L/2}^{L/2}\frac{1}{\eta_k}\mathrm{d}X, \tag{5.3}$$

which implies that the first term in (5.2) is also negative. Thus, the quadrature expression for the mean kinetic energy for layer k, up to terms of order $O(\epsilon^4)$,

$$T_k = c^2\frac{h_k\rho_k}{2\,L}\left[\int_{\alpha_0-A}^{\alpha_0}\frac{3+R(\zeta,\boldsymbol{C})}{\eta_k\sqrt{R(\zeta,\boldsymbol{C})}}d\zeta - 1\right], \tag{5.4}$$

is positive definite. Here the parameters $\boldsymbol{C}(\alpha)$ are evaluated at $\alpha = \alpha_0$, the position of the crest—a root of the nonlinear equation (4.6)—and depend on the speed c and the amplitude A (which determines the position of the root $\alpha_0 - A$ of $R(\zeta, \boldsymbol{C}) = 0$ corresponding to the trough).

This expression of the kinetic energy, together with the expression for the potential energy (3.4), allow us to test the resilience of the equipartition of energy for our class of periodic waves as the amplitude increases. This property is well known to hold for infinitesimal amplitude waves (Yih 1959), and we show below, when direct comparisons with Euler solutions are presented, that this property in fact depends strongly on period for both model and Euler solutions, in agreement with the finding of Holyer (1979) for the different set-up of doubly infinite depths.

5.4. *Limits of validity of the strongly nonlinear model*

Our goal is to determine regions within the domain of existence of periodic solutions of the strongly nonlinear model where we can expect good agreement with Euler solutions. We expect this agreement to be satisfactory when the long-wave assumption at the basis of the asymptotic model is satisfied in each layer. Let $d_k = \max(\eta_k)$ denote the maximum thickness of layer k, ($k = 1, 2$) and λ a characteristic wavelength. A condition that would ensure that the long-wave assumption holds in both layers is

$$\max(d_1, d_2)/\lambda \ll 1.$$

Thus, to establish a validity criterion, we need an *a priori* estimate of a characteristic horizontal length scale as well as upper bounds for the thickness of each layer. Once again, the limiting positions corresponding to the foliating solitary waves β_d and β_e prove to be useful.

First, we focus on the quasilinear regime. For the region within the domain of existence where $\beta_d/A > 1/2$ and $|\beta_e|/A > 1/2$, the positions of the crest and trough of the periodic wave solutions are far from the corresponding limiting positions and quasi-symmetrical with respect to the interface, which translates in an almost-sinusoidal wave shape. The maximum layer thickness is therefore well approximated by $d = \max(h_1 + A/2, h_2 + A/2)$. Furthermore, the dispersion relation for infinitesimal waves (relation (3.42) in Choi & Camassa 1999) offers a reasonable approximation for the dependence of the period on the phase speed for periodic solutions; hence, a good estimate for the horizontal length scale is half the period of the infinitesimal waves with speed c. Note that the dispersion relation of the two-layer model no longer agrees with the dispersion relation of Euler equations (Lamb 1932, p. 231) when the long-wave parameter d/λ is not sufficiently small (see e.g. figure 2.12 of Tiron 2009 for typical errors in speed of the model with respect to Euler predictions). Thus, by using the discrepancy between Euler and model dispersion relation, we can infer a

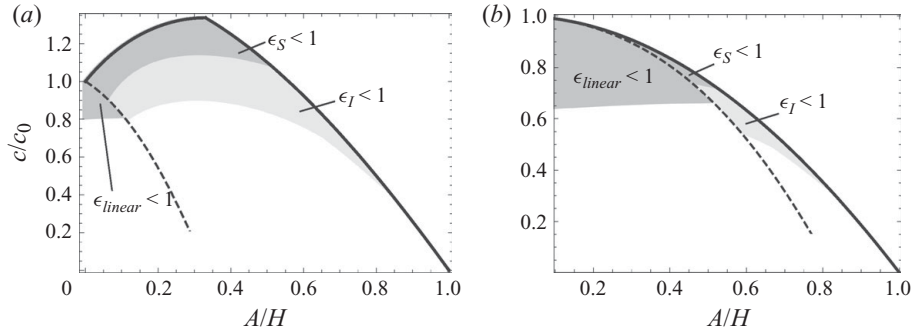

FIGURE 9. Regions in the domain of existence where we can expect a good agreement of the solutions of the strongly nonlinear model with Euler solutions for the configurations from figures 8(*a*) and 8(*b*), respectively. The region at the left of the dashed line contains solutions with quasi-sinusoidal wave shapes, whereas for the region at the right the periodic solutions approach the foliating family β_d.

threshold long-wave parameter that isolates the region of validity of the strongly nonlinear model from this first part of the domain.

For the region within the domain of existence where $\beta_d/A < 1/2$ (or $|\beta_e|/A < 1/2$), the position of the crest (or the position of the trough) of periodic solutions approaches the limiting position β_d (or β_e). In this case, the maximum layer depth is well approximated by $d = \max(h_2 + \beta_d, h_1 - \beta_d + A)$ (or $d = \max(h_1 - \beta_e, h_2 + \beta_e + A)$) whereas the characteristic horizontal length scale of the foliating solitary waves provides a good estimate for the horizontal length scale of periodic solutions since the wave shapes are comparable. Obvious candidates for a characteristic length scale of solitary waves are the effective wavelength λ_I and the ratio between the amplitude and the maximum slope of the interface ($\lambda_S = A/\max[\zeta_X]$). An analytical expression for the effective wavelength in terms of elliptic functions has been derived by Choi & Camassa (1999) in the case of solitary waves with no currents at infinity. Relationships for effective wavelength corresponding to solitary waves on general currents at infinity are reported by Tiron (2009, see table 1, Appendix A), and a strategy for computing the maximum slope of solitary waves and fronts is outlined in Appendix A; see (A 9). We can thus define two long-wave parameters based on the effective wavelength and the maximum slope, respectively,

$$\epsilon_I = d/\lambda_I, \quad \epsilon_S = d/\lambda_S. \tag{5.5}$$

The condition $\epsilon_S \ll 1$ measures the local validity of the solutions and therefore is a much more restrictive criterion than $\epsilon_I \ll 1$, which is an average of the steepness of the profile with respect to the thickness of the layer. We thus expect that for $\epsilon_I \ll 1$ and $\epsilon_S \sim O(1)$ to have a reasonable overall agreement with Euler solutions, while locally the model predicted profile does not match the Euler solution. We note that in the limit to fronts, however, the effective wavelength diverges to infinity, the only measure of a characteristic horizontal length scale being provided by the maximum slope criterion. We summarize these ideas in figure 9, where we depict the regions in the domain of existence of periodic solutions when the long-wave parameter is smaller than unity.

We remark that some of the validity regimes we have identified could follow the classification of two-layer asymptotic models provided by Bona *et al.* (2008); however, we have not pursued this analysis here and work strictly with our model

within their 'shallow-shallow' configuration. In this context, it is worth mentioning that the strongly nonlinear model seems to work rather well (but not always) even outside this configuration.

6. Validation of the model by comparison to Euler solutions

In this section, we compare periodic solutions of zero horizontal momentum in each layer obtained by the strongly nonlinear model against numerical solutions of the full Euler system under the same constraints. As remarked above, because of (3.13), this also implies that the layer horizontal momenta are zero for both model and Euler solutions. We first concentrate on the parent two-layer Euler system, using the algorithm based on boundary integrals documented by Grue *et al.* (1999) and Rusås (2001). Convergence properties of this algorithm have been extensively studied in these references and others. We have performed further tests in the context of the present work within our constrained class. We have adapted this algorithm to seek solutions of a prescribed mean elevation, which requires a continuation search on the initial guesses for this iterative algorithm (the details of this continuation procedure are not important here and will be reported elsewhere). In particular, we focus here on the practical limitations of the asymptotic model in view of the validity estimates of § 5.4, by testing the model with this class of periodic waves as well as their limiting forms of solitary waves and fronts, in various parametric regimes. Of course, the two-layer set-up is highly idealized. In order to assess the relevance of this idealization, we next compare periodic solutions of Euler equations for continuous (but still near two-layer) stratification, obtained with a variant of the algorithm of Turkington, Eydeland & Wang (1991), by looking at relevant diagnostics such as wave profile and fluid velocities.

6.1. *Two-layer Euler system versus strongly nonlinear model*

For a given density ratio ρ_r between the two layers, the subcritical and supercritical regimes ($h_r < \sqrt{\rho_r}$ and $h_r > \sqrt{\rho_r}$, respectively) will have many similarities, with the sole exception being the 'polarity' of the waves. As pointed out before, this is reflected in the tendency of the crests or troughs, respectively, to flatten first with increasing amplitude. The critical case, on the other hand, is special and deserves a separate study. Accordingly, in the next two sections we report results from the subcritical and critical cases only.

6.1.1. $h_r < h_{critical}$

First, we look at a subcritical configuration $h_r < h_{critical} \equiv \sqrt{\rho_r}$, whose speed versus amplitude chart is illustrated in figure 8(*a*). The corresponding chart with several constant period curves computed with the full Euler two-layer system is reported in figure 10, where the regions of validity discussed in the previous section are identified by shaded portions of the existence domain.

Some general features of the comparison between strongly nonlinear model and the full Euler solutions emerge from this figure. First, both strongly nonlinear and Euler models share the presence of two types of period isolines – isolines along which the phase speeds are subcritical $c < c_0$ and isolines that have a portion on which the phase speeds are supercritical $c > c_0$. As one can see from figure 10, the agreement between model and Euler predictions is, in general, superior in the region where the phase speeds are supercritical (and the period is larger).

Next, the discrepancy between model and Euler period isolines amplifies with increasing amplitude, this tendency being enhanced by decreasing period. While the

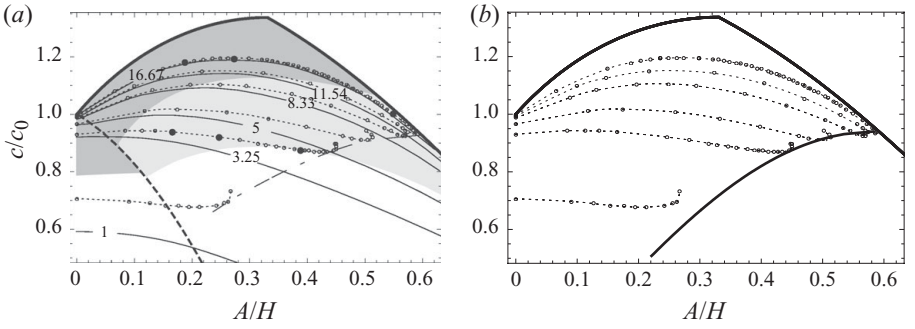

FIGURE 10. (*a*) Isolines of period (labelled with L/H) for the configuration from figure 8(*a*); Continuous line denotes strongly nonlinear model, and dotted line and data points denote Euler solutions. The dash-dotted curve marks the limiting amplitude, inferred from the numerical results obtained with the Euler code, before overhanging develops. The shaded areas are the estimated regions of validity of the strongly nonlinear model; see figure 9(*a*). (*b*) Slope level set curve for foliating solutions and Euler period isolines, corresponding to the slope angle of approximately 40°. The model tracks the location of the envelope from the numerically computed Euler isolines for most of the domain of expected validity.

model isolines wrap on the right boundary of the existence domain (corresponding to the branch of fronts) as the amplitude increases, Euler isolines reach a maximum amplitude and overturn, which correspond to periodic wave profiles of the overhanging nature (multiple-valued interface for given x-locations) reported in the literature in different set-ups (either infinite depth fluids or front solutions, see e.g. Meiron & Saffman 1983 and Turner & Vanden-Broeck 1985, respectively). Prolonging the constant period isolines past the overturning seems to lead to periodic waves of smaller amplitude and larger speed with deeper overhangs, until this process terminates with a wave of a self-intersecting profile of extreme form; see figure 11(*a–d*). (These overhanging features resemble those computed by Pullin & Grimshaw (1988) for solitary waves with one infinite fluid layer.) We remark that this process of termination by self-intersection can only be conjectured at this point and may not apply to long-period waves, where we have not been able to achieve convergence of the Euler code. Moreover, this process may not apply to the infinite depth case, see Turner & Vanden-Broeck (1985). We further remark that both subcritical and supercritical period isolines overturn in the region of subcritical phase speeds, and that the size of the overturning region decreases with increasing period. The phenomenon of overhanging periodic waves is connected with the existence of a maximum-amplitude, single-valued Euler wave profile for a given period. The envelope of constant period isolines for subcritical speeds defines a maximum amplitude boundary for single-valued solutions of two-layer Euler equations; see the dash-dotted curve in figure 10(*a*). It is remarkable that the strongly nonlinear model, for which all periodic solutions are naturally single valued, still manages to inform about this envelope through the setting of a threshold for model validity based on the slope achieved along the proper foliating solutions (computed with (A 9)) in the existence domain; see figure 10(*b*).

Another important feature of the Euler solutions emerges from this plot, namely the non-uniqueness of periodic waves of given amplitude and speed. As can be seen from figure 10(*a*), there exists a set of points in the parameter space (A, c) at the left of the dash-dotted curve, where at least two Euler solutions, one regular whose

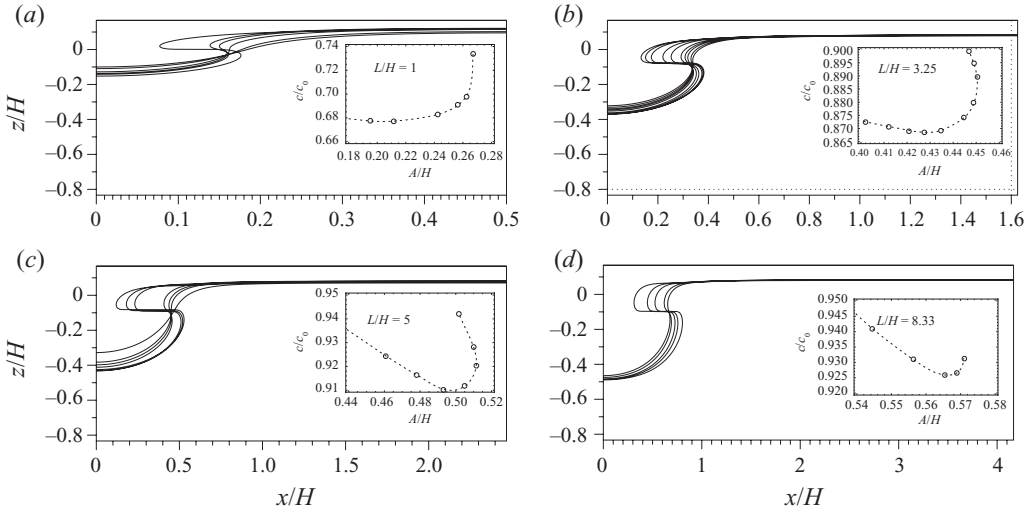

FIGURE 11. (*a–d*) Euler solutions of near maximal amplitude along four period isolines from figure 10. The period and the corresponding pairs amplitude–speed are marked in the insets.

profile is a single-valued graph of x and one multiple-valued of the overhanging type, move at the same speed with the same amplitude (but with different periods).

In figure 12, we compare the Euler solutions against model predictions for the points marked in figure 10(*a*). In particular, in figure 12 we also provide the wave profiles from KdV model solutions for identical parameters as both (*a*) and (*b*), for the lowest and largest amplitude waves. As expected, there are notable differences as amplitude increases with respect to the strongly nonlinear model, and, of course, with the corresponding Euler profiles. Note also that while the strongly nonlinear model fails to give local agreement with Euler solutions, it nonetheless succeeds in capturing their broadening at extrema of the interface for increasing amplitudes with large periods (similar to what is observed with solitary waves).

The progressive breakdown of the strongly nonlinear model's fidelity is captured reasonably well from the effective wavelength criterion discussed in the previous section. The condition $\epsilon_S \ll 1$ isolates the level sets of period predicted by the model which best match the Euler level sets. However, note that the strongly nonlinear model performs well even in regions where $\epsilon_S \sim O(1)$ provided the long-wave parameter based on effective wavelength ϵ_I is much smaller than unity. Also note that for all period isolines of the model, the wave shapes are steepening and converging to a front of amplitude H with the 'effective' wavelength $(h_r/(h_r+1))\,L$ selected by mass conservation. This horizontal length scale is a good estimate for the effective wavelength of both model and Euler wave profiles; see figures 13 and 14. Finally, figure 15 presents a comparison between model results and Euler results for the mean kinetic and potential energies. In particular, one can clearly see the equipartition of kinetic and potential energies for small-amplitude waves for both strongly nonlinear and full Euler solutions.

6.1.2. $h_r = h_{critical}$

For a configuration corresponding to the critical depth ratio, the domain of existence of solutions of the strongly nonlinear model contains only subcritical speeds $c < c_0$,

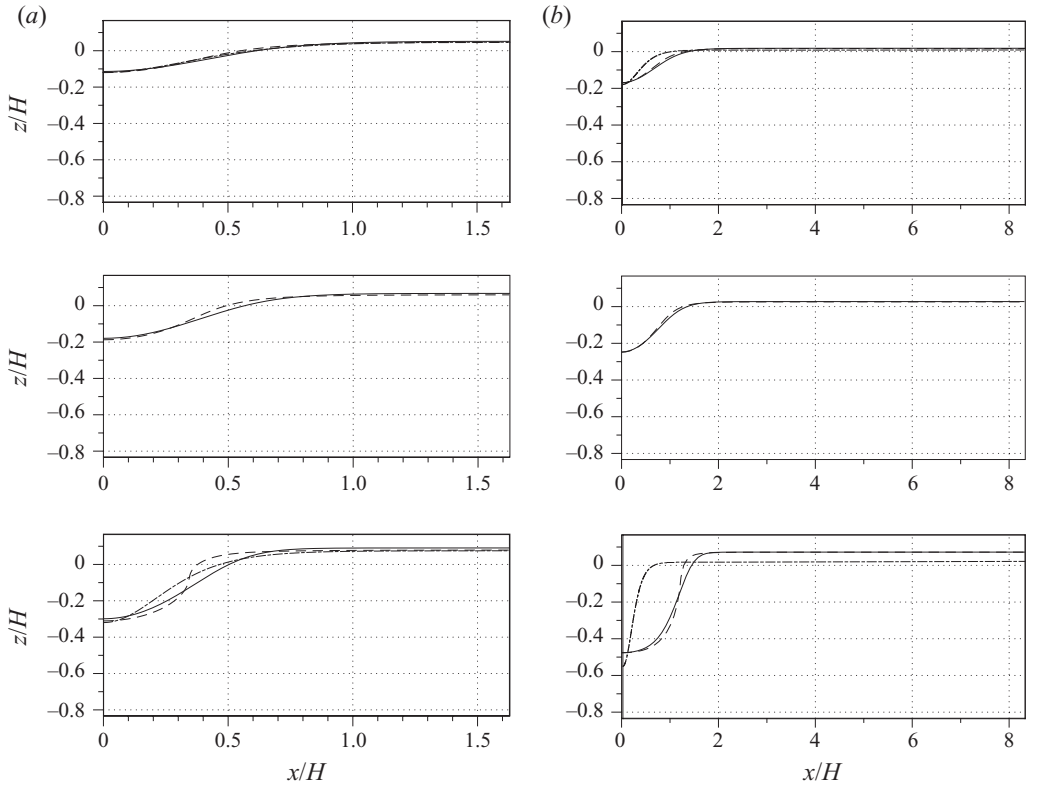

FIGURE 12. Comparison between Euler solutions (dashed line), strongly nonlinear model (continuous line) and KdV (dot-dashed line) solutions corresponding to the points marked in figure 10, for (*a*) $L/H = 3.25$ and (*b*) $L/H = 16.67$, respectively.

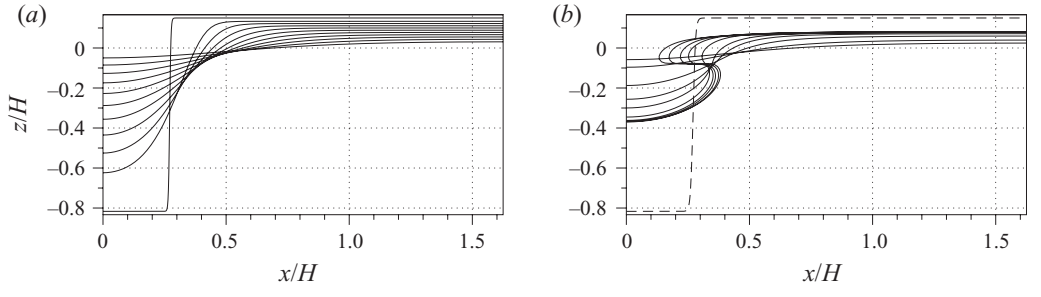

FIGURE 13. Wave shapes on an isoline of period $L/H = 3.25$. (*a*) Model, (*b*) Euler (the dashed line reports the model-predicted limiting front with speed zero and amplitude H from (*a*)).

and the only limiting forms of periodic waves consist of fronts. In this instance, the quasi-linear region (where the wave shapes are quasi-sinusoidal) occupies a larger portion of the domain of existence; see figure 16(*a*). As expected, the agreement of the strongly nonlinear model with Euler is superior in the regions with $\epsilon_S \ll 1$. Note that when the period increases, the isolines of period wrap along the front branch of the domain of existence of the strongly nonlinear model solutions, which confirms that the front branch represents an actual branch of front solutions for

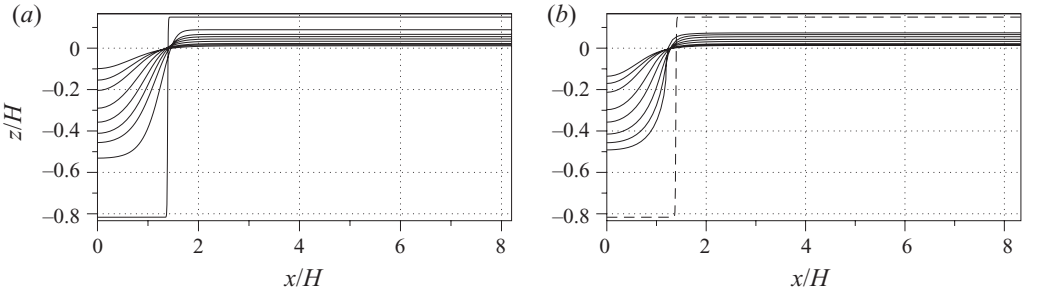

FIGURE 14. Same as figure 13 for $L/H = 16.67$.

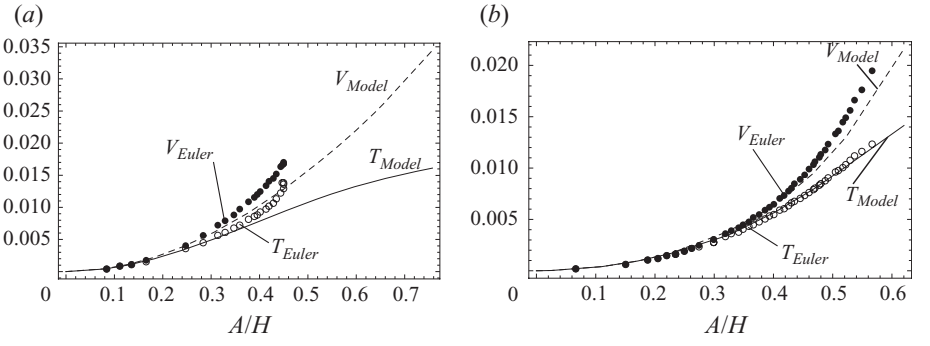

FIGURE 15. Mean kinetic energy (continuous line denotes strongly nonlinear model and circles denote Euler solutions) and mean potential energy (dashed line denotes strongly nonlinear model and dots denote Euler solutions) on two isolines of period from figure 10: (*a*) $L/H = 3.25$ and (*b*) $L/H = 16.67$, respectively. The energies are non-dimensionalized with γH^2.

the full Euler equations. We remark that these fronts are not the 'classical' fronts studied by Dias & Vanden-Broeck (2003), given that in our case the two layers are in relative uniform motion at both left and right asymptotic states. In figure 16(*b–d*), we compare the Euler wave shapes corresponding to points on the front branch to front solutions of the strongly nonlinear model, by matching the zero crossing points of the profiles. The agreement is quite reasonable even when ϵ_S is of order $O(1)$.

6.2. *Continuous stratification Euler system versus strongly nonlinear model*

We complete the study of our class of periodic waves with a limited comparison of results of the two-layer strongly nonlinear model with periodic wave solutions of Euler equations with continuous stratification with a finite, albeit small, pycnocline thickness. We note that the limit to zero thickness has been studied by James (2001). Stationary periodic solutions for continuous stratification are determined by using an iterative scheme based on the one described by Turkington *et al.* (1991). This algorithm solves the Dubreil–Jacotin–Long (DJL) equation through minimization of kinetic energy for prescribed potential energy with respect to a background density stratification. Figure 17(*a*) depicts the density field for a periodic wave solution obtained with this algorithm, with background continuous stratification consisting of two layers of constant density, separated by a thin diffused interface corresponding to experimentally measured physical parameters (cf. Grue *et al.* 1999).

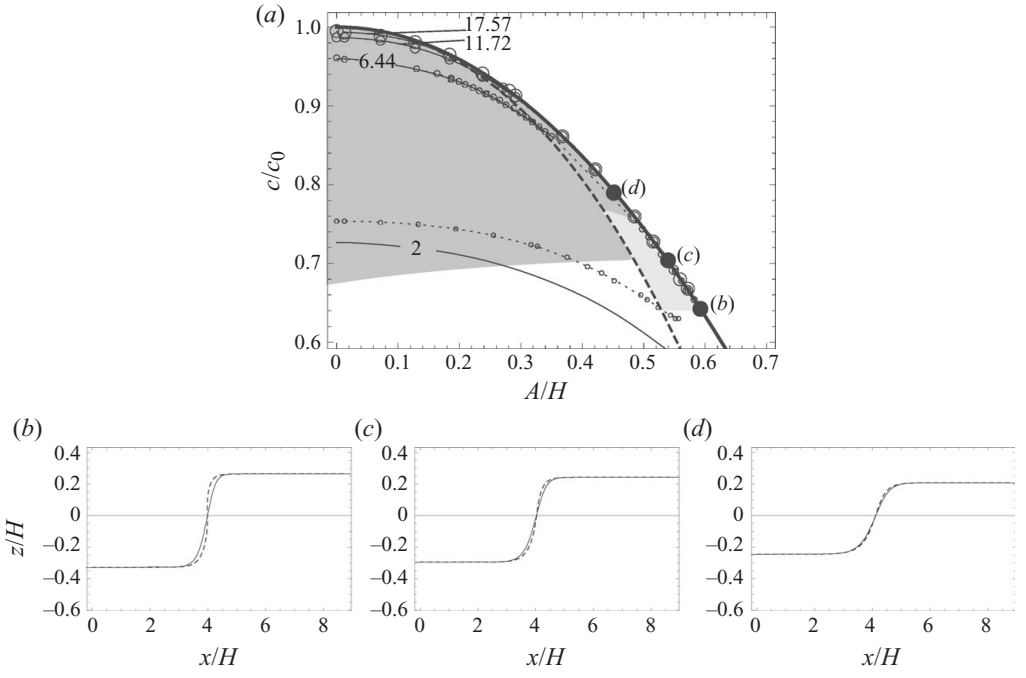

FIGURE 16. (*a*) Isolines of period (labelled with L/H) for the configuration from figure 8(*c*); Continuous line denotes strongly nonlinear model, and dotted line and data points denote Euler solutions. The dashed curve corresponds to $\beta_d/A = 1/2$ whereas the shaded areas are the regions of validity of the strongly nonlinear model; see figure 9(*b*). (*b–d*) Dashed line denotes Euler periodic solutions (half profile) with period $L/H = 17.56$ and with speed and amplitude corresponding to the points marked in figure 16(*a*); continuous line denotes front solution of the strongly nonlinear model with the same speed and amplitude. The profiles are horizontally aligned at the mean level crossing points.

Following the strategy outlined by Tiron (2009, chapter 3), we determine a two-layer configuration that approximates the continuous stratification by optimizing with respect to critical speed, mass and potential energy of a reference equilibrium state, which is determined to be the mean level of the continuously stratified solution. In figure 17(*b*) we compare the density isoline corresponding to the mean density 1.0105 g cm^{-3} with the interface predicted by the optimized strongly nonlinear model. Figure 17(*c*) compares the self-induced horizontal shear at the maximum displacement of the pycnocline with the horizontal velocity profiles predicted by the strongly nonlinear model asymptotics, through the reconstructed z-dependence of the velocity field provided by (2.9). We remark that our implementation of the DJL solver, while allowing for the volume flux to be set to zero, does not impose the constraint of zero horizontal momentum for the resulting solution. However, for the solution shown here as well as for most of the ones we have studied in this algorithm, the momentum evaluated diagnostically after their computation turns out to be very close to zero.

7. Discussion

We have presented a study of finite-depth periodic travelling wave solutions of a strongly nonlinear model for internal wave propagation in two-layer inviscid,

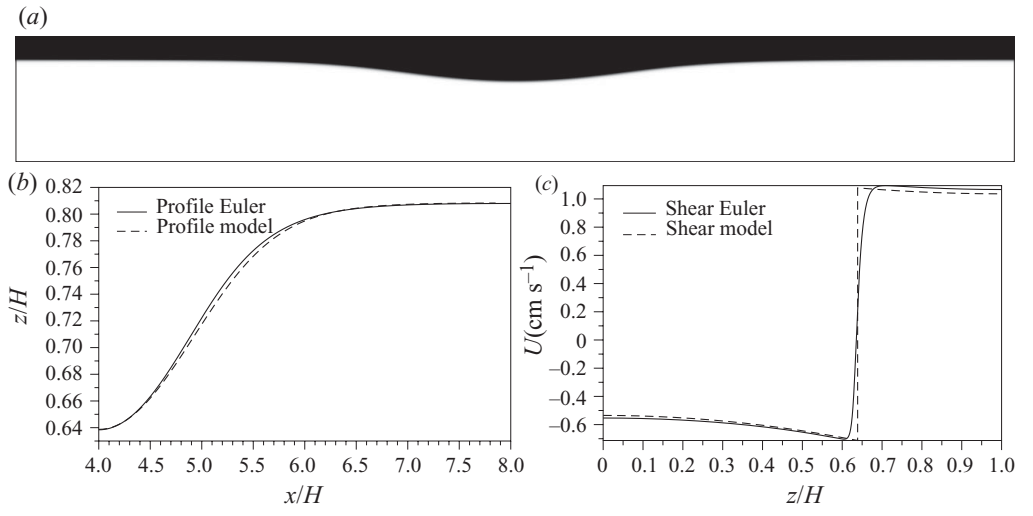

FIGURE 17. (*a*) Density field for a periodic wave in continuous stratification, $L/H = 8$. (*b*) Wave profile comparison. (*c*) Horizontal velocity shear at the wave trough. The background density profile is $\overline{\rho}(z) = \rho_{min} + (1/2)(\rho_{max} - \rho_{min})(1 - \tanh(\sigma z))$, with $z \in [-h_2, h_1]$. Physical parameters are $h_1 = 15$ cm, $h_2 = 62$ cm, $\sigma = 1.03$, $\rho_{min} = 0.999$ g cm^{-3}, $\rho_{max} = 1.022$ g cm^{-3}. The available potential energy per unit length for this wave is 581.635 g cm s^{-2}.

incompressible fluid systems. These solutions constitute a much richer class than their limiting forms, such as solitary wave solutions, which have been the main focus of previous model investigations in both theory and experiments. In contrast with these limiting forms, the lack of an asymptotic spatial reference state opens up additional parametric freedom, and the distinction of which parameter subsets constitute solutions relevant for physical situations becomes less clear. With our study we have provided some order in the various results established in the literature on two-layer finite-depth periodic internal wave solutions, by examining in detail the role of the physical constraints on such waves and by studying their transition to the limiting infinite-period forms. In particular, we have shown how such solutions constitute a five-parameter family, which we conjecture holds for the general two-layer Euler periodic single-valued solutions of symmetric type. Moreover, we have provided examples that show non-uniqueness within this family, associated with 'overhanging' (multiple-valued) solutions of the Euler system.

In this work, we have chosen to focus on the particular parametric subset corresponding to waves that generate no horizontal period-averaged momentum in each layer, with respect to some inertial reference frame defined to be that of the laboratory. Additionally, we impose that these waves maintain a prescribed period average interface height, which can be thought of as that of an undisturbed reference state. We chose these constraints with a past asymptotic temporal reference state in mind, in which the process of wave generation proceeds from a quiescent state with well-defined uniform layer thicknesses, in closed (but long) domains with wave generators that do not apply a net horizontal force. While these conditions do not necessarily guarantee the exact enforcement of our choice of constraints, it is plausible to assume that under these circumstances our two sets of constraints can be approximately satisfied. True periodicity could be approximated by a section of the wavetrain far from both the generation region and the leading wave region,

where the displaced interface connects with the flat surface between undisturbed fluids. Other parametric subsets have been proposed in the literature for Euler and weakly nonlinear systems. We looked at some of them in the context of our model in Appendix C.

Several results have emerged from our study. First, we have identified analytically the domain of existence of the periodic waves in the two-parameter space of amplitude and speed. The boundary of this domain is represented by the limiting curves of speed versus amplitude of solitary waves and fronts. While the solitary wave branch is a long-wave approximation to the corresponding full two-layer Euler branch (but practically indistinguishable from it as shown in the previous work of Camassa *et al.* 2006), the front branch is exact and coincides with that of the full Euler system, as we show in Appendix A. Thus, the domain of existence we have identified thanks to the model informs us on the corresponding domain for the full Euler system, even though not every existing model solution within the domain can be expected to be a good approximation of an Euler solution.

The numerical solutions of the full Euler two-layer system have also brought forth the feature of overhanging periodic waves of higher speed than single-valued waves of the same amplitude, within the same class of constrained zero momenta and volume fluxes for solutions for the strongly nonlinear model. Similar overhanging solutions of Euler equations have been the subject of previous studies; however, most of these have concentrated on the case of infinite thickness of either both or one fluid layer. In contrast, our study has concentrated on finite depth of both layers, and in particular we locate the domain of existence of overhanging periodic solutions for these configurations. Moreover, our Euler solutions explore the transition from finite period to infinite period front solution of the overhanging type. It is interesting to speculate that the point at which the envelope of maximum amplitudes for given period intersects the boundary of the existence domain along the front branch separates this branch between single-valued front profiles and overhanging ones similar to those found by Dias & Vanden-Broeck (2003). If so, it is remarkable that the model maximum slope curves can offer an estimate of this transition amplitude along the front branch.

By comparing with numerical solutions of the full Euler system, we have shown that the model solutions are accurate approximations whenever certain criteria of asymptotic accuracy based on definitions of 'long-waveness' and departure from near-linear regimes are satisfied. This first and most stringent application of these criteria excludes from the existence domain the region where overhanging waves are found, and the model predictions are very good approximations of the full Euler solution. It is remarkable that with a second criterion based on a non-local definition of effective wavelength, the model is still able to pick up with some accuracy the location of flattening crests and/or troughs, even though the wave profile may fail to offer a good local approximation. In particular, the Euler computations show that a portion of the existence domain from the model needs to be removed as Euler solutions do not exist in this region. Euler periodic waves of the constrained class we have studied have a (single-valued regular) wave of maximum amplitude for a given period. The envelope of all the constant period curves in the (A, c) plane gives rise to a curve marking the boundary of existence of these Euler periodic solutions. Here again the model is able to inform about the boundary of this region by examining the maximum slope curve of its solutions in the existence domain.

A large portion of the existence domain is taken by periodic waves which are *de facto* the spatially truncated version of solitary waves or fronts. These are not

the classic cases of such internal waves, which are asymptotic to quiescent states. Instead, these infinite-period limiting waves are defined on background relative currents between the two layers. This situation has not been given much attention in previous work, presumably due to lack of physical interest for a velocity jump to be sustained over an infinite interface. However, the length of this interface becomes finite when clipped in the process of constructing periodic waves, thus justifying the sketch of such limiting cases presented in Appendices A and B.

A result of possible relevance in applications, where solitary waves rarely occur in true solitary fashion and are more commonly members of wave trains with multiple crests, is exhibited by the supercritical speed region near the vertex of the existence domain. There, for a fixed supercritical speed and relatively long period waves, two different amplitude waves exist, with one attaining an amplitude that can be substantially larger than the maximum wave which is the limit of the classic solitary wave branch to a front.

Several future directions could stem from our study of the periodic solutions for the two-layer strongly nonlinear model. Perhaps the one most physically relevant is the modulated wavetrains that can be obtained perturbatively by allowing the quadrature integration constants to be slowly varying functions of space and time. To this end, asymptotics of the quadrature formula for nearly flat crests or troughs would have to be established and are in progress. Such a study would be of relevance in geophysical applications, where near-solitary wave trains are a common occurrence. On a more mathematical level, the overhanging solutions and their model approximations provide a starting point to explore the issue of multiplicity for this class of two-layer Euler solutions (as well as their stability properties) and criteria (Amick & Turner 1986) of selection between the alternatives of vertical tangency or broadening to front solutions in the solitary wave limits.

R. C. and R. T. gratefully acknowledge support from NSF through DMS-0509423 and CMG-0620687. R. T. would also like to acknowledge a summer internship at the Center for Nonlinear Studies of Los Alamos National Laboratory, supported by the US Department of Energy, where this work was initiated. The authors would like to thank Cory Hauck and Jie Yu for helpful discussions, and gratefully acknowledge Wooyoung Choi's comments and feedback to an earlier version of the manuscript. Last but not least, we thank one of the referees for bringing several relevant references to our attention.

Appendix A. Solitary waves on uniform layer currents

Closed form solutions for solitary waves in the most physically common situation of fluid at rest at infinity can be found for the strongly nonlinear model (Choi & Camassa 1999). The analysis can easily be extended to the situation of layers of inviscid fluid in relative uniform motion. This set-up is admittedly less likely to have physical relevance, (but note Gavrilov 1994 for immiscible fluids) as a (constant) velocity jump cannot be sustained indefinitely as $|x| \to \infty$ by real viscous fluids; however, this investigation is relevant in the discussion of various classes of periodic waves, where velocity jumps occur locally within the period. Interfacial waves between two layers in uniform-current relative background motion have been studied in the periodic case for unbounded fluids by Saffman & Yuen (1982) using weakly nonlinear models and numerical computations of Euler equations. In this appendix, we summarize the properties of solitary waves on relative currents which are relevant

to the study in § 4 (see Tiron 2009 for a detailed analysis, Makarenko & Maltseva 2007 and Makarenko, Maltseva & Kazakov 2009 where similar results are reported).

A.1. *Quadrature and domain of existence*

Throughout this appendix, we shall work in the frame of reference of the waves, i.e. that of an observer who sees the wave profile as constant in time. We will thus study the two-parameter family of solitary wave solutions on a given reference state (determined by the 'hardware' parameters of heights and densities of the undisturbed layers h_1, h_2 and ρ_1, ρ_2, respectively), parametrized by the uniform currents at infinity in each of the two layers $\widehat{u}_1|_\infty, \widehat{u}_2|_\infty$. We introduce the non-dimensional parameters

$$\rho \equiv \rho_1/\rho_2, \qquad h \equiv h_1/h_2,$$

and note the relationships between the total height $H = h_1 + h_2$ and the widths of the layers

$$h_1 = \frac{hH}{1+h} \qquad \text{and} \qquad h_2 = \frac{H}{1+h}. \tag{A 1}$$

Let $\widehat{u}_k|_\infty$, $k = 1, 2$ denote the arbitrary currents at infinity in the wave frame, and let U_k be the square of these speeds $U_k \equiv \widehat{u}_k^2|_\infty$, $k = 1, 2$ (i.e. $U_k = (gH)F_k^2$, where F_k are layer Froude numbers).

By using the appropriate boundary conditions at infinity, the quadrature (2.8) becomes

$$\zeta_X^2 = 3\gamma \frac{\zeta^2\left[\zeta^2 + q_1(U_1, U_2)\zeta + q_2(U_1, U_2)\right]}{\rho_1 h_1^2 U_1 \eta_2 + \rho_2 h_2^2 U_2 \eta_1}, \tag{A 2}$$

where

$$q_1(U_1, U_2) = \frac{1-h}{1+h}H + \frac{\rho U_1 - U_2}{(1-\rho)g}, \qquad q_2(U_1, U_2) = -\frac{h}{1+h}H^2 + \frac{H(\rho U_1 + hU_2)}{g(1-\rho)(1+h)}. \tag{A 3}$$

Solitary wave solutions exist only for certain combinations of currents in the two layers. First, we observe that the root of the denominator in (A 2),

$$a_*(U_1, U_2) = \frac{h}{1+h}\frac{\rho h U_1 + U_2}{U_2 - \rho h^2 U_1}H\,, \tag{A 4}$$

is, in general, outside the physical domain except the limiting cases $U_1 = 0$ or $U_2 = 0$, when a_* equals h_1 or $-h_2$, respectively. Thus, the domain of existence of solitary waves in the quadrant for positive U_1 and U_2 can be determined by looking at the behaviour of the roots of the quadratic $\zeta^2 + q_1(U_1, U_2)\zeta + q_2(U_1, U_2)$ on lines

$$U_2(\kappa) = \kappa U_1, \qquad \text{with} \qquad \kappa \in [0, \infty).$$

It is found that solitary wave solutions exist for

$$U_1 \in [U_{1min}(\kappa), U_{1max}(\kappa)],$$

with $U_{1min}(\kappa)$ as the root of equation $q_2(U_1, \kappa U_1) = 0$,

$$U_{1min}(\kappa) = \frac{(1-\rho)h}{(1+h)(\rho + h\kappa)}gH, \tag{A 5}$$

corresponding to a dispersive wave of infinitesimal amplitude and with infinite period, and

$$U_{1max}(\kappa) = U_1^{(1)}(\kappa) = (1-\rho)\frac{(\sqrt{\rho} - \sqrt{\kappa})^2}{(\kappa - \rho)^2}gH, \tag{A 6}$$

corresponding to an internal bore solution. The amplitudes of the solitary waves along the line $U_2 = \kappa U_1$ for $U_1 \in [U_{1min}(\kappa)\,, U_{1max}(\kappa)]$ vary between zero and

$$a_{max}(\kappa) = \frac{h\sqrt{\kappa} - \sqrt{\rho}}{(1+h)(\sqrt{\kappa} + \sqrt{\rho})} H, \tag{A 7}$$

having the sign given by the sign of $a_{max}(\kappa)$. We thus have

$$a(U_1, \kappa U_1) = \frac{-q_1(U_1, \kappa U_1) - \mathrm{sgn}(h\sqrt{\kappa} - \sqrt{\rho})\sqrt{\Delta(U_1, \kappa U_1)}}{2}, \tag{A 8}$$

where $\Delta(U_1, U_2) = q_1(U_1, U_2)^2 - 4q_2(U_1, U_2)$. Note that the (right) boundary of the domain of existence corresponding to fronts, parametrized by

$$(U_{1max}(\kappa), \kappa U_{1max}(\kappa)) \quad \text{with} \quad \kappa \in [0\,, \infty),$$

where $U_{1max}(\kappa)$ is given by (A 6) and the corresponding amplitude by (A 7), represents exact conjugate state solutions of Euler equations; see Tiron (2009) for details. We also remark that the validity of each solitary wave solution in the domain of existence can be tested by computing the associated long-wave parameter based on maximum slope (or, alternatively, on effective wavelength); see relation (5.5). By the quadrature formula, the maximum slope of the wave profile can be computed explicitly by chain rule and solving for the inflection point with positive slope, $\zeta = \zeta_I$. Hence

$$\max \zeta_X = \sqrt{R(\zeta_I)} \quad \text{with} \quad \partial_\zeta R(\zeta_I) = 0\,. \tag{A 9}$$

Finally, it should be mentioned that an alternative (geometric) approach based on the criticality of two-layer uniform current flows by Bridges & Donaldson (2007), and utilizing the same motion invariants of mass and momentum flux (or flow-force) and Bernoulli differential constant, seems to offer a strategy for the determination of the parametric space of solitary wave existence summarized here and analysed in detail by Tiron (2009). In this context, we note the existence results by Mielke (1995) directly on the Euler set of equations shed further light on the solitary-wave-on-currents problem.

Appendix B. Solitary waves in 'artificial' parameters

The domain of existence in the parameter space $(\beta\,, c)$ of solitary waves with the prescribed fluxes (4.11) can be found by fixing β and determining the range of speeds c for which solitary waves with property (4.11) exist.

From (4.11), with $\eta_k|_\infty = h_k + (-1)^k\beta$, we can determine the current at infinity in the wave frame in each layer

$$\widehat{u}_1|_\infty = -\frac{ch_1}{h_1 - \beta}, \quad \widehat{u}_2|_\infty = -\frac{ch_2}{h_2 + \beta}. \tag{B 1}$$

Note that for obtaining the range of phase speeds c for fixed β, we can mirror the discussion in Appendix A by shifting the heights of the asymptotic level as $|X| \to \infty$

$$h_1 \equiv h_1 - \beta\,, \quad h_2 \equiv h_2 + \beta\,, \quad h \equiv (h_1 - \beta)/(h_2 + \beta)), \tag{B 2}$$

and study solitary waves on currents parametrized by

$$U_1 = \frac{c^2 h_1^2}{(h_1 - \beta)^2}, \tag{B 3}$$

on a line in the parameter space (U_1, U_2) given by

$$U_2 = \kappa U_1 \qquad \text{with} \qquad \kappa = \frac{h_2^2(h_1-\beta)^2}{h_1^2(h_2+\beta)^2}. \tag{B 4}$$

Thus, by using (B 1)–(B 4), we can express the coefficients of the quadratic at the numerator of the quadrature q_1, q_2 and the root at the denominator a_* solely in terms of c and β; see Tiron (2009). Based on the results in Appendix A and by using (B 1)–(B 4), we can infer that solitary wave solutions with the property (4.11) for fixed β exist for

$$c \in [c_{min}(\beta), c_f(\beta)],$$

where relationships (A 5) and (A 6) for the speed of the limiting cases of solitary and front solutions turn into

$$c_{min}(\beta) = \sqrt{\frac{\gamma(h_1-\beta)^3(h_2+\beta)^3}{\rho_1 h_1^2(h_2+\beta)^3 + \rho_2 h_2^2(h_1-\beta)^3}}, \tag{B 5}$$

and

$$c_f(\beta) = \sqrt{g(1-\rho_r)H}\,\frac{(h_1-\beta)(h_2+\beta)}{\sqrt{\rho_r}h_1(h_2+\beta)+h_2(h_1-\beta)}, \tag{B 6}$$

respectively. The corresponding maximum amplitude is given by (A 7) modified by the new β-shifted asymptotic heights

$$a_f(\beta) = \frac{(h_1-\beta)^2 - h_r\sqrt{\rho_r}(h_2+\beta)^2}{(h_r\sqrt{\rho_r}-1)\beta + h_r\sqrt{\rho_r}h_2 + h_1}. \tag{B 7}$$

As in Appendix A, the polarity of the family of solitary waves parametrized by β is given by the sign of the amplitude of the front (B 7). We thus have, from (B 7),

$$a_f(\beta) < 0 \text{ for } \beta < \beta_0 \text{ and } a_f(\beta) > 0 \text{ for } \beta > \beta_0,$$

with

$$\beta_0 = \frac{H}{1+h_r}\,\frac{h_r - \sqrt{h_r\sqrt{\rho_r}}}{1+\sqrt{h_r\sqrt{\rho_r}}}. \tag{B 8}$$

The amplitude of the foliating family of solitary waves parametrized by β is therefore

$$a(c\,;\beta) = \frac{-q_1(c\,;\beta) + \operatorname{sgn}(\beta_0-\beta)\sqrt{\Delta(c\,;\beta)}}{2}, \qquad c \in \left[c_{min}(\beta), c_f(\beta)\right]. \tag{B 9}$$

We can eliminate β from (B 7) as root of the quadratic equation that is in the range $[-h_2, h_1]$,

$$\beta_f(a) = -\frac{a}{2} + \frac{h_1(\sqrt{\rho_r}+1)}{1-h_r\sqrt{\rho_r}} - \frac{\sqrt{a^2(1-h_r\sqrt{\rho_r})^2 + 4H^2h_r\sqrt{\rho_r}}}{2(1-h_r\sqrt{\rho_r})}, \tag{B 10}$$

and substituting in (B 6) we obtain an explicit formula for the amplitude–speed relation for the front branch subject to restriction $h_r\sqrt{\rho_r} \neq 1$

$$c_f(a) = \sqrt{Hg}\,\frac{(1+h_r)\sqrt{1-\rho_r}}{(h_r\sqrt{\rho_r}-1)^2}\left(h_r\sqrt{\rho_r}+1-\sqrt{\left(\frac{a}{H}\right)^2(h_r\sqrt{\rho_r}-1)^2+4h_r\sqrt{\rho_r}}\right). \tag{B 11}$$

For the special depth ratio $h_r\sqrt{\rho_r} = 1$ the above expression becomes invalid. In this case the dependence of a_f on β is linear and (B 7) becomes

$$a_f(\beta) = h_1 - h_2 - 2\beta\,, \tag{B 12}$$

with the maximum speed (B 6) for this case being

$$c_f(\beta) = \sqrt{Hg}\frac{(1+h_r)^2}{h_r}\sqrt{\frac{1-\sqrt{\rho_r}}{1+\sqrt{\rho_r}}}\frac{(h_1-\beta)(h_2+\beta)}{H^2}\,. \tag{B 13}$$

The front branch amplitude–speed relation in this special case $h_r\sqrt{\rho_r} = 1$ is therefore

$$c_f(a) = \sqrt{Hg}\frac{(1+h_r)^2}{4h_r}\sqrt{\frac{1-\sqrt{\rho_r}}{1+\sqrt{\rho_r}}}\left(1-\left(\frac{a}{H}\right)^2\right)\,. \tag{B 14}$$

We note that the front branch $c_f(a)$ is symmetric with respect to c axis; the level β corresponding to $a_f = 0$ is given by β_0.

Finally, we note how a simple geometric construction based on the effective wavelength can give an approximate speed-amplitude relation for a given period, based on the observation that actual periodic solutions are very close to their limiting foliating solution if the period is sufficiently large. In fact, equating the area in the strip of height β and width L to the area under the solitary wave profile $2A\lambda_I$, gives, because of the fast exponential decay of solitary waves, the position β and speed c corresponding to a mean-zero elevation, period-L wave in the constrained class. For a configuration of periodic waves approaching solitary waves of depression, this is determined by

$$\frac{\beta L}{2} = \frac{2}{\mu(\beta, A)}\left[\sqrt{a_*(\beta) - a_-(\beta, A)}\,(F(\delta, k) - E(\delta, k)) + \sqrt{\frac{A\,a_*(\beta)}{a_-(\beta, A)}}\right]\,, \tag{B 15}$$

where the modulus and argument of the elliptic functions depend on β and A through

$$k^2 = \frac{A + a_*(\beta)}{a_*(\beta) - a_-(\beta, A)}, \quad m^2 = \frac{a_-(\beta, A)}{A}\frac{a_*(\beta) + A}{a_-(\beta, A) - a_*(\beta)}, \quad \sin\delta = \frac{1}{m}.$$

Here $a_*(\beta)$ is the root at the denominator of the quadrature, and $a_-(\beta, A) = A - q_1(c(\beta, A); \beta)$. We can obtain an explicit dependence of c on β and A by imposing that $\zeta = -A$ is a root of the quadratic $\zeta^2 + q_1(c;\beta)\zeta + q_2(c;\beta)$ and thus obtain a linear equation in c^2. This construction is illustrated in figure 18.

Appendix C. Other classes of periodic waves

In this appendix, we review a few alternatives of our choice of constraints as well as models reported in the literature for periodic wave motion in a two-layer system of finite depth. These alternatives all share with our model the assumption of single-valuedness of the interface between the two layers, thereby excluding overhanging wave solutions. With this functional assumption, the minimal number of quantities needed to determine a unique wavetrain is five for all cases, just as in our study of the strongly nonlinear model.

We remark that the majority of these alternative studies are aimed at the limiting forms of periodic waves corresponding to solitary waves on zero currents at infinity, the issue of the possible generation mechanisms of periodic wave trains thus being circumvented. These alternatives leave the mean position of the interface

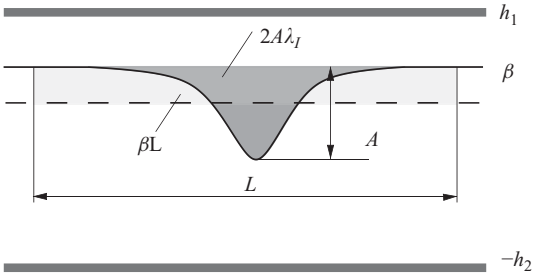

FIGURE 18. Sketch of the approximation for periodic wave solutions close to their solitary wave limit. The crest position β of a periodic solution for given amplitude (a) and period L can be determined by equating the area under the foliating solitary wave profile with the area above the mean level over a period L.

a priori undetermined, and seek some other constraints fixing the five quantities that determine the periodic wavetrain. In the following, we show how to cast these different constraints in the framework of the strongly nonlinear model.

C.1. *Periodic waves with prescribed volume fluxes*

Miyata (2000) proposed the same strongly nonlinear long-wave model and studied a class of periodic waves that limit on solitary waves on zero current at infinity. The position of the crest is located at fixed distance h_2 from the bottom wall (thus at distance $h_1 = H - h_2$ from the top wall). The volume fluxes in each layer are set to zero in a particular frame of reference which is designated as the 'lab' frame, so that in the wave frame they are $\widehat{Q}_k = -ch_k$, $k = 1, 2$, where c is the phase speed. Thus, Miyata obtains a two-parameter family of periodic solutions parametrized by the phase speed c and amplitude A, which, in the limit of infinite period, recovers the solitary wave solution with asymptotic behaviour at infinity $\eta_k \to h_k$ and zero current in both layers.

These constraints (fixed position of the trough and zero volume fluxes in each layer) yield a distinct class of waves with respect to the one we have concentrated on and defined in § 4 (waves of momentum zero in the frame for which the total volume flux is zero). While the total volume flux in the lab frame is zero for this particular class of waves,

$$Q = \eta_1 \overline{u}_1 + \eta_2 \overline{u}_2 = 0\,, \tag{C 1}$$

the total horizontal momentum is different than zero since

$$I_1 + \rho_r I_2 = 0 \neq I_1 + I_2\,. \tag{C 2}$$

Miyata derived his periodic solutions for the particular depth ratio $h_r \equiv h_1/h_2 = 1/\sqrt{\rho_r}$, which is different than the critical case $h_r = \sqrt{\rho_r}$. For this particular ratio, his periodic solutions are expressible via elliptic functions.

We can cast Miyata's solutions in our notation in the general case (for arbitrary h_r), by looking at the class of waves for which the position of the trough is not constrained. Again, the strongly nonlinear model yields solutions which are expressible via hyperelliptic functions except for the particular case $h_r\sqrt{\rho_r} = 1$, when the root in the denominator for the quadrature (2.8) vanishes and the hyperelliptic integral associated with the quadrature degenerates into an elliptic integral. In addition to generalizing Miyata's class of periodic waves, we will also determine their domain of existence following a similar strategy as for our main constrained class of periodic solutions. We remark that by not enforcing the mean position of interface constraint,

the analysis is greatly simplified for Miyata's class with respect to that of our main class.

Following the same procedure as in § 4, the constants C_3 and C_4 can be determined uniquely by imposing the conditions that 0 and $-A$ are roots of the polynomial at the numerator in (2.8). Thus

$$C_3 = \frac{c^2}{2}\left[\frac{\rho_1 h_1}{h_1 + A} - \frac{\rho_2 h_2}{h_2 - A}\right] + \frac{\gamma A}{2}, \quad C_4 = C_3 h_1 + c^2 \frac{\rho_1 h_1 + \rho_2 h_2}{2}. \tag{C 3}$$

With all the constants C_i, $i = 1, \ldots, 4$, thus determined, we can construct the periodic solution from the quadrature (2.8) and determine the domain of existence of this class of periodic waves in the parameter space c and A. We restrict our attention to the case $h_1 < h_{critical}$. Once again, there are two bounding curves for this domain, which correspond to limiting cases of solitary waves with the prescribed fluxes. One limiting branch consists of the 'classic' solitary waves that satisfy the asymptotic condition, $\eta_k \to h_k$ and $\overline{u}_k \to 0$ as $|X| \to \infty$. The other limiting branch is given by solitary waves of opposite polarity superimposed on different non-zero currents at infinity (since the position of the interface at infinity in this case is $(h_1 + A, h_2 - A)$), which can be determined by imposing the flux condition in each layer

$$(\overline{u}_k - c)\,\eta_k = (\overline{u}_k|_\infty - c)(h_k + (-1)^k A) = -c h_k, k = 1, 2. \tag{C 4}$$

Using the notation from Appendix A yields

$$U_1 = \frac{c^2 h_1^2}{(h_1 + A)^2}, \quad U_2 = \frac{c^2 h_2^2}{(h_2 - A)^2}. \tag{C 5}$$

The coefficients q_1, q_2, given by (A 3), respectively, in the quadratic polynomial from the numerator of (A 2) can be thus expressed in terms of A and c. For a given amplitude A, we want to determine the velocity c of the solitary wave on the current U_1, U_2 given by (C 5). That is equivalent to requiring that A is the root of the equation

$$A^2 + q_1(A, c)A + q_2(A, c) = 0,$$

which determines the square of the phase speed c^2,

$$c(A)^2 = \gamma\left(\frac{\rho_1 h_1}{(h_1 + A)^2} + \frac{\rho_2 h_2}{(h_2 - A)^2}\right)^{-1}. \tag{C 6}$$

In order to select from the curve (A, c) given by (C 6) the part that corresponds to actual solitary waves, we need to make sure that the second root of the equation

$$r^2 + q_1(A, c(A))r + q_2(A, c(A)) = 0,$$

say B, satisfies the condition $B > A$. Thus, we need the condition

$$q_1 = -(A + B) < -2A.$$

This yields

$$-\frac{\rho_2 h_1 h_2}{(h_2 - A)^2} + \frac{\rho_1 h_1 h_2}{(h_1 + A)^2} < 0,$$

which allows us to conclude that relation (C 6) defines the branch *II* of the limiting solitary waves for

$$A > |a_m| = \left|\frac{h_2 - \sqrt{\rho_r} h_1}{\sqrt{\rho_r} + 1}\right|,$$

where a_m is the maximum amplitude of the usual front for layer thicknesses (h_1, h_2). We remark that solutions of Miyata's class effectively take a different constraint surface through the five-dimensional parameter space of periodic solutions, and that the domain of existence on these surfaces coincides with our main class along the segments of boundary corresponding to the classical solitary wave solutions and the axes. We also remark that the critical depth ratio case follows a similar fate as that of our main constrained class, namely the classic solitary wave branch at the top of the existence domain shrinks to the point $(0, c_0)$ and only the type *II* solutions survive.

C.2. *Periodic waves with prescribed mean Eulerian velocities*

Funakoshi & Oikawa (1986) studied the two-layer Euler system numerically and computed a class of periodic waves under the constraint that the period average of the Eulerian wall velocity (defined in the lab frame) be zero for both top and bottom walls. Their other two constraints are to fix the position of the crest and the period length (thus fixing five independent parameters, phase speed, two mean Eulerian wall velocities, crest position and period).

Similar to the previous sections, we now use the strongly nonlinear model to find how these different constraints relate to the quadrature constants C_i, $i = 1, \ldots, 4$. By fixing the position of the crest of the wave, we specify one of the four roots in the polynomial at the numerator (2.10), say r_2, which constitutes a constraint among the integration constants C_i, $i = 1, \ldots, 4$, or $P(r_2, \boldsymbol{C}) = 0$, where P is the polynomial in the numerator of (2.8). By fixing the period, we obtain another integral constraint involving the constants C_i, $i = 1, \ldots, 4$, $L = \mathscr{L}(\boldsymbol{C})$; see relation (3.2). By using the asymptotic expressions (3.17) for the mean Eulerian velocities and setting them to zero for both layers, we obtain two more integral constraints for the constants $C_1, \ldots, C_4$ involving the wave speed (c) $\widetilde{u}_k(c, \boldsymbol{C}) = 0$, $k = 1, 2$. We remark that a given wave shape in the class of § 4 may not be a solution of the class of these constraints, and certainly not with the same phase speed because the kinetic energy equation (3.18) with mean Eulerian wall velocity zero in each layer yields

$$T_k = c\, I_k/2, \tag{C 7}$$

so that the horizontal momenta I_k must be non-zero, unlike the constraint imposed in § 4. The question of whether the same wave profile (but different phase speeds) can belong to both classes might be interesting but lies outside of the present study.

C.3. *Weakly nonlinear unidirectional limit*

Among the class of periodic solutions that can be constructed for two-layer systems, a special mention goes to those derived through weakly nonlinear, unidirectional models. Funakoshi & Oikawa (1986) also derived a KdV–mKdV equation for waves of small amplitude, whence periodic solutions of standard elliptic functional form derive. However, we remark that this particular class of waves does not recover the correct asymptotic limit of the dispersion relation (as evidenced by figure 9*b*,*c* in that paper).

In fact, an asymptotically consistent KdV–mKdV model is a particular case of a unidirectional model that can be obtained from the strongly nonlinear model. This reduction of degrees of freedom for the wave motion, from bi- to unidirectional, has the effect of reducing the number of parameters that define a periodic wavetrain from five to three. We can thus anticipate that the constraints that rely on the definition of a lab frame (through its connection to wave speed) for the full Euler two-layer system as well as for the strongly nonlinear model will be violated, in general, albeit possibly only by asymptotically small errors arising from the unidirectional limit process.

The travelling wave solution ansatz in the unidirectional model in Choi & Camassa (1999) ((A 14) in Appendix A) results in the quadrature formula

$$\zeta_X^2 = \frac{c_3}{4(c_4 - c_5)} \frac{\zeta^4 + \dfrac{2}{3}\dfrac{c_1}{c_3}\zeta^3 + \dfrac{2(c_0 - c)}{c_3}\zeta^2 + C_1\zeta + C_2}{\zeta + \dfrac{c_2 c_1 + (c_0 - c)(2c_4 - c_5)}{2c_1(c_5 - c_4)}}, \tag{C 8}$$

where C_1 and C_2 are constants of integration which are related to purely geometric wave properties such as amplitude, period, and mean level, while c_1, c_2, c_3, c_4 and c_5 are 'hardware' constants determined by the densities and layer thicknesses (Choi & Camassa 1999, (A 7*a*) and (A 7*b*) in Appendix A). The quadrature (C 8) has the same structure as its bi-directional analogue (2.8), but only two constants of integration are needed. While we have not extensively studied this class here, it is interesting to note that at least for small-amplitude wavetrains, well within the range of validity of the unidirectional model, its periodic solutions are in good agreement with those of the bi-directional model in the constrained class of zero period-averaged momentum for each layer.

REFERENCES

Amick, C. J. & Turner, R. E. L. 1986 A global theory of internal solitary waves in two-fluid systems. *Trans. Amer. Math. Soc.* **298**, 431–460.

Benjamin, T. B. 1995 Verification of the Benjamin–Lighthill conjecture about steady water waves. *J. Fluid Mech.* **295**, 337–356.

Benjamin, T. B. & Lighthill, M. J. 1954 On Cnoidal waves and bores. *R. Soc. Lond. Proc.* A **224**, 448–484.

Bona, J. L., Lannes, D. & Saut, J.-C. 2008 Asymptotic models for internal waves. *J. Math. Pures Appl.* **89**, 536–566.

Bridges, T. J. & Donaldson, N. M. 2007 Reappraisal of criticality for two-layer flows and its role in the generation of internal solitary waves. *Phys. Fluids* **19**, 072111.

Camassa, R., Choi, W., Michallet, H., Rusås, P.-O. & Sveen, J. K. 2006 On the realm of validity of strongly nonlinear asymptotic approximations for internal waves. *J. Fluid Mech.* **549**, 1–23.

Choi, W. & Camassa, R. 1996 Weakly nonlinear internal waves in a two-fluid system. *J. Fluid Mech.* **313**, 83–103.

Choi, W. & Camassa, R. 1999 Fully nonlinear internal waves in a two-fluid system. *J. Fluid Mech.* **396**, 1–36.

Craig, W., Guyenne, P. & Kalisch H. 2005 Hamiltonian long-wave expansions for free surfaces and interfaces. *Commun. Pure Appl. Math.* **58**, 1587–1641.

Dias, F. & Vanden-Broeck, J.-M. 2003 On internal fronts. *J. Fluid Mech.* **479**, 145–156.

Drociuk, R. J. 2004 On the closed form solution for the geodesics in SdS space. *ArXiv General Relativity and Quantum Cosmology e-prints*, arXiv:gr-qc/0402093.

Duda, T. F., Lynch, J. F., Irish, J. D., Beardsley, R. C., Ramp, S. R., Chiu, C.-S., Tang, T. Y. & Yang, Y. J. 2004 Internal tide and nonlinear internal wave behaviour at the continental slope in the northern South China Sea. *IEEE J. Ocean Eng.* **29**, 1105–1131.

Funakoshi, M. & Oikawa, M. 1986 Long internal waves of large amplitude in a two-layer fluid. *J. Phys. Soc. Japan* **55**, 128–144.

Gavrilov, N. V. 1994 Internal solitary waves and smooth bores which are stationary in a laboratory coordinate system. *J. Appl. Mech. Tech. Phys.* **35**, 29–33.

Green, A. E. & Naghdi, P. M. 1976 A derivation of equations for wave propagation in water of variable depth. *J. Fluid Mech.* **78**, 237–246.

Grue, J., Jensen, A., Rusås, P.-O. & Sveen, J. K. 1999 Properties of large-amplitude internal waves. *J. Fluid Mech.* **380**, 257–278.

Helfrich, K. & Melville, K. 2006 Long nonlinear internal waves. *Annu. Rev. Fluid Mech.* **38**, 395–425.

Holyer, J. Y. 1979 Large amplitude progressive interfacial waves. *J. Fluid Mech.* **93**, 433–448.

Klopman, G. 1990 A note on integral properties of periodic gravity waves in the case of a non-zero mean Eulerian velocity. *J. Fluid Mech.* **211**, 609–615.

Koop, C. G. & Butler, G. 1981 An investigation of internal solitary waves in a two-fluid system. *J. Fluid Mech.* **112**, 225–251.

James, G. 2001 Internal travelling waves in the limit of a discontinuously stratified fluid. *Arch. Ration. Mech. Anal.* **160**, 41–90.

Lamb, H. 1932 *Hydrodynamics*, 6th edn. Cambridge University Press.

Longuet-Higgins, M. S. 1975 Integral properties of periodic gravity waves of finite amplitude. *R. Soc. Lond. Proc.* A **342**, 157–174.

Makarenko, N. I. & Maltseva, Zh. L. 2007 Phase velocity spectrum of internal waves in a weakly-stratified two-layer fluid. *Fluid Dyn.* **2**, 278–294.

Makarenko, N. I., Maltseva, Zh. L. & Kazakov, A. Yu. 2009 Conjugate flows and amplitude bounds for internal solitary waves. *Nonlinear Process. Geophys.* **16**, 169–178.

McIntyre, M. E. 1981 On the 'wave momentum' myth. *J. Fluid Mech.* **106**, 331–347.

Meiron, D. I. & Saffman, P. G. 1983 Overhanging interfacial gravity waves of large amplitude. *J. Fluid Mech.* **129**, 213–218.

Mielke, A. 1995 Homoclinic and heteroclinic solutions in two-phase flow. In *Proceedings of the IUTAM/ISIMM Symposium on Structure and Dynamics of Nonlinear Waves in Fluids* (ed. A. Mielke & K. Kirchgässner), pp. 353–362. World Scientific.

Miyata, M. 1985 An internal solitary wave of large amplitude. *La Mer* **23**, 4348.

Miyata, M. 1988 Long internal waves of large amplitude. In *Nonlinear Water Waves, IUTAM Symp.* (ed. K Horikawa & H Maruo), pp. 399–406. Springer.

Miyata, M. 2000 A note on broad narrow solitary waves. *PRC Report 00-01,* SOEST 00-05, 1–26.

Monismith, S. G, Cowen, E. A., Nepf, H. M., Magnaudet, J. & Thais, L. 2007 Laboratory observations of mean flows under surface gravity waves. *J. Fluid Mech.* **573**, 133–147.

Pullin, D. I. & Grimshaw, R. H. J. 1988 Finite-amplitude solitary waves at the interface between two homogeneous fluids. *Phys. Fluids* **31**, 3550–3559.

Rusås, P.-O. 2001 On nonlinear internal waves in two- and three-layer fluids. DSc thesis, Department of Mathematics, University of Oslo.

Saffman, P. G. & Yuen, H. C. 1982 Finite amplitude interfacial waves in the presence of a current. *J. Fluid Mech.* **123**, 459–476.

Su, C. H. & Gardner, C. S. 1969 Korteweg–de Vries equation and generalization III: derivation of the Korteweg–de Vries equation and Burgers equation. *J. Math. Phys.* **10**, 536–539.

Thorpe, S. A. 1968 On the shape of progressive internal waves. *Phil. Trans. R. Soc. Lond.* A. **263**, 563–614.

Tiron, R. 2009 Strongly nonlinear internal waves in near two-layer stratifications: generation, propagation and self-induced shear instabilities. PhD thesis, Mathematics Department, University of North Carolina.

Troy, D. & Koseff, J. R. 2005 The instability and breaking of long internal waves. *J. Fluid Mech.* **543**, 107–136.

Turkington, B., Eydeland, A. & Wang, S. 1991 A computational method for solitary internal waves in a continuously stratified fluid. *Stud. Appl. Math.* **85**, 93–127.

Turner, R. E. L. & Vanden-Broeck, J.-M. 1985 The limiting configuration of interfacial gravity waves. *Phys. Fluids* **29**, 372–375.

Williams, J. M. 1981 Limiting gravity waves in water of finite depth. *Phil. Trans. R. Soc. Lond.* A. **263**, 139–188.

Yih, C.-S. 1959 Gravity waves in a stratified fluid. *J. Fluid Mech.* **8**, 481–508.

Yih, C.-S. 1997 The role of drift mass in the kinetic energy and momentum of periodic waves and sound waves. *J. Fluid Mech.* **331**, 429–438.